Vienna University of Technology

Master's Thesis

Hysteresis in the AKT signaling pathway

Martin E. Fürst
Wigandgasse 18
3400 Klosterneuburg

supervised by
Dr. Gerhard Schütz, Institut für Angewandte Physik, TU Wien
Dr. David Gomez Míguez, Universidad Autonoma de Madrid

January 19, 2016

Contents

Acknowledgements

The research work for this thesis was performed during an Erasmus exchange semester in the beautiful city of Madrid. It was therefore subsidized by the European Union, which I am grateful for.

Firstly, I would like to express my gratitude to Professor David Gomez Míguez for accepting a stranger to his lab and allowing me to work with him. His expertise, kindness and guidance made research an enjoyable experience for me.

Also, I want to thank my colleagues in Madrid: Adriana Sanz for all her help and patience in the lab and Victoria Lucía Doldán for lively discussions on the project.

Finally, I have to thank Professor Gerhard Schütz for his support of me doing this thesis in a foreign lab, his good humor, his incredibly fast replies and especially for introducing me to the field of biophysics. Without his knowledge and enthusiasm in sharing it, I would have never discovered this fascinating area of research.

Abstract

Life and function of eukaryotic cells are governed by metabolic and signaling pathways. These pathways are constituted by a multitude of organic molecules. Many of these systems exhibit highly nonlinear behavior, caused by different combinations of feedback loops, feedforward loops et cetera. Possible behaviors include bistability, hypersensitivity, robustness and complex dose-response-curves. These circumstances increase the difficulty of designing drugs for e.g. cancer treatments and predicting their effectiveness. In a recent study, D.G. Miguez observed an inverted hysteresis loop when treating the AKT-pathway with the small-molecule inhibitor ZSTK ([32]). The main objective of this thesis was to build a biologically sound, mathematical model to understand the observed behavior. Furthermore, we tried to reproduce the experiments using a different method.

Chapter 1

Introduction

"How can unstable molecules stably store information?" ([26])

The sentence above is taken from a research paper from John E. Lisman from 1985 ([26]). Biologists observed processes that – once triggered – continued irreversibly, despite the short lifetime of the involved molecules and the initial stimulus. Lisman proposed a simple mechanism (basically consisting of a positive feedback loop) to explain how long-term memory of neuronal cells might work. Instead of utilizing any permanent "inscriptions", Lisman claimed the "wiring" of the molecules to be responsible.

Since then, molecular biologists have identified many biomolecules and their relationships and it is now commonly accepted that bistable signaling pathways provide a mechanism for permanent change in a cell and for irreversibility of processes (e.g. cell division, frog metamorphosis ([10])).

Today, cellular signaling pathways are also thought to play a key role in many types of cancer ([27],[37],[38],[19],[15]). Therefore, also commercial interest in signaling pathways arises from their importance when developing drugs. Highly nonlinear signaling pathways are a potential source of failure in drug treatment. Nonlinearities can cause phenomena such as bistability, hypersensitivity, robustness, schedule-dependent activity and complex dose-response-curves ([31]).

One of the most studied nonlinear signaling cascades is the AKT pathway, a frequent mutational target in cancer ([3], [30]). These mutations result in constitutive activation of the pathway, driving uncontrolled cell proliferation and resistance to apoptosis. At the core of the pathway is the serine/threonine kinase AKT, a signaling hub that phosphorylates many downstream effectors involved in cell growth and survival, cell cycle regulation, stress resistance,

apoptosis, metastasis and insulin signaling ([18]). The architecture of the AKT pathway presents several main self-regulatory loops ([6]): A negative feedback loop via mTOR and an autocatalytic loop via IRS1. AKT activation can be measured by monitoring the translocation to the cytoplasm of its direct target FoxO1a, a member of the Forkhead family of transcription factors involved in cell cycle progression ([20]).

In a yet unpublished study ([32]), FoxO1a translocation is used to study the influence of the nonlinear self-regulation of AKT in response to pathway inhibition. The study found a peculiar dose-response relationship when treating 786-O cells with the small-molecule inhibitor ZSTK. This thesis is aimed at exploring whether the observed behavior can be explained as resulting from the architecture of the pathway – the "wiring" of the molecules – or if additional elements are necessary.

Chapter 2 is intended to give an overview of the biological background of the studied system. The chapter introduces the concept of receptors, feedback loops and pathways. It also discusses in more detail the workings and the constituents of the AKT signaling pathway.

Chapter 3 provides the reader with an introduction to the required mathematical tools for studying cellular signaling pathways.

The Materials and Methods employed while working on this thesis are documented in chapter 4. This includes the numerical methods and the experimental procedures.

Chapter 5 presents the results of the work performed for the thesis. It is split in two parts: Presentation of the mathematical model and its numerical evaluation, and presentation of the immunofluorescence experiments.

In chapter 6, the results are interpreted and discussed. Also, an outlook is given on how the project could be continued.

Finally, the appendix features the detailed lab protocols, a list of figures and the bibliography.

Chapter 2

Biological Background

2.1 Intracellular signal transduction

In the evolution of life as we know it today, communication between cells is a prerequisite for the forming of multi-cellular organisms. However, a prerequisite for cell-to-cell communication is the development of intracellular mechanisms to interpret extra-cellular signals. These mechanisms already evolved in unicellular organisms. In most cases, the reception of signals depends on *receptor proteins* located on the cell surface. These receptor proteins bind the signal molecule, which activates the receptor, triggering one or multiple *intracellular signaling pathways*. Such a signaling pathway consists of a number of molecules (again, mainly proteins, therefore *intracellular signaling proteins*) that are subsequently activated. At the end of such a *signaling cascade*, so called *effector proteins* then alter the cell behavior by affecting gene regulation, ion channels, metabolic pathways or parts of the cytoskeleton ([1]).

2.1.1 Receptors

Even though there are signal molecules that do bind to *intra*cellular receptors, most extracellular signal molecules bind to receptor proteins on the surface of the target cells ([1] pg. 891). The majority of these receptor proteins belong to one of three classes:

- Ion-channel-coupled receptors
- G-protein-coupled receptors
- Enzyme-coupled receptors

Out of these three classes, the third type is the relevant type for the presented work. These receptors transduce signals to the interior of a cell by either including a catalytic domain themselves or by binding to an enzyme within the cell. The majority of these enzymes are kinases, with *Tyrosine Kinases* being the most numerous. Enzyme-coupled receptors that activate (or form) tyrosine kinases are referred to as *Receptor Tyrosine Kinases* or RTKs. The AKT-signaling pathway starts with the activation of an RTK.

After the extracellular signal molecule (the *first messenger*) has been bound to its respective receptor, the signal is further relayed within the cell via *intracellular signaling molecules*.

2.1.2 Intracellular signaling molecules

Intracellular signaling molecules are divided into *small* and *large* intracellular signaling molecules. The small molecules are also referred to as *second messengers* and they typically spread the signal by diffusing to other parts of the cell. Important examples are cyclic AMP and Ca2+.

The large molecules are proteins and they typically relay the signal by activating the next signaling protein or effector proteins ([1] pg. 894). In most cases, this activation happens via the gain or loss of phosphate groups. A large class of proteins switches between its on- and off-states by phosphorylation via a *protein kinase* and de-phosphorylation via a *protein phosphatase*. The activity of the involved kinases and phosphatases may itself be controlled by other kinases and phosphatases. These would then form a *signaling cascade* in which the original signal is relayed throughout the cell, amplified and often branched to different signaling pathways. AKT is also known as *protein kinase B*, indicating its function within the AKT-pathway.

To some signals, cells respond very smoothly while to other stimuli they might react very abruptly (in a highly non-linear way). Such behavior may be caused by e.g.

- Cooperativity: Some enzymes require the simultaneous binding of multiple signaling molecules to be activated. (PKA requires 4 molecules of cAMP, for example, see [1] pg. 900)
- Simultaneous inhibition: If one signaling molecule activates the enzyme catalyzing a reaction and at the same time inhibits an enzyme catalyzing the opposite reaction, the response will also be sharpened.

- Feedback loops: When the output of a process regulates that same process, we talk about a feedback loop. Feedback loops are capable of creating true all-or-none responses. For this reason, they are of special interest for this thesis and will therefore be discussed in more detail below.

2.1.3 Feedback loops

Whenever the output of a process regulates that same process, we will talk about a feedback loop. In *negative feedback*, the output inhibits its own production whereas in *positive feedback*, the output stimulates its own production ([1] pg. 901). Unfortunately, this nomenclature is *not* perfectly universal. In some texts, negative feedback refers to any feedback that influences inhibitors and in some texts, negative feedback refers to any feedback that increases (subjectively) undesirable effects.

Sufficiently strong positive feedback loops can give rise to switch-like behavior of a signaling pathway. This means, that the output of the process remains at a high level even though the initial stimulus is removed. Switch-like behavior is essential for stable cell decisions, such as cell division or cell differentiation ([11]).

In cellular signaling, feedback loops are typically formed by a whole cascade of signaling molecules that influence each other's activity either positively or negatively. With an even number of negative regulation, the overall feedback loop is a positive feedback loop; the most often discussed example being *double-negative feedback* (see e.g. [11]).

A more general review of feedback and how it can give rise to switch-like behavior will be given in the Mathematics chapter (see 3). This chapter will now introduce in more detail the AKT signaling pathway.

2.2 The AKT-pathway

As mentioned in the introduction (chap. 1), the PI3-Kinase-AKT-pathway plays a central role in promoting survival and growth of many cell types. This chapter is dedicated to provide more details on which molecules form the pathway and how they interact.

AKT activation primarily promotes cell survival, proliferation and growth ([42]). These are the main consequences of AKT overexpression in cancer. Other effects of AKT activation include angiogenesis and an increased cellular

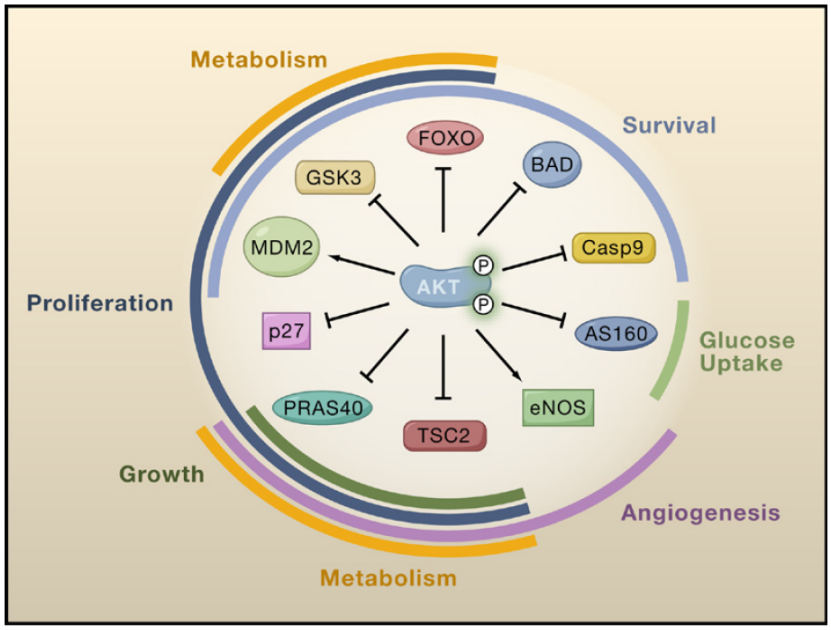

Figure 2.1: An overview of ten AKT substrates. AKT-mediated phosphorylation leads to activation (arrows) or inhibition (blocking arrows) of these molecules, resulting in the effects shown.(Figure from [30]).

metabolism rate (increased glucose uptake) ([30]). Figure 2.1 depicts the cellular targets of AKT responsible for the mentioned effects.

The AKT signaling cascade is a highly nonlinear pathway. Hyperactivation leads to insulin resistance, uncontrolled cell proliferation and metastasis, as well as enhanced resistance to drug treatment ([18]). AKT serves as a hub for multiple cell decisions and is indirectly regulated by the balance between the kinase PI3K and the phosphatase PTEN.

There are over 100 reported non-redundant AKT substrates ([30]), resulting in the various effects described above. We will here focus on the pathway upstream of AKT, on the signaling cascade that activates AKT.

The pathway is affected by a negative regulatory loop employing the mTOR-raptor complex. There are also several positive regulatory loops acting on AKT (see [31] pg. 91).

2.2.1 The main constituents

IGF-receptor and IRS1

The insulin-like growth factor 1 receptor (IGF-1 receptor) is a transmembrane receptor that belongs to the class of tyrosine kinase receptors.

The *Insulin Receptor Substrate 1* (IRS1) is the linking molecule between exterior signal and intracellular signaling pathway. IRS1 contains a pleckstrin homology domain (PH-domain) and a phosphotyrosine-binding domain (PTB-domain) and is located at the intracellular leaf of the plasma membrane. Activation of the cell-surface receptor recruits IRS1 to the membrane and IRS1 subsequently promotes the recruitment and activation of PI3K ([4]).

PI3K and ZSTK

Phosphoinositide 3-kinase (PI3K) is a heterodimeric lipid kinase composed of a regulatory (p85) and a catalytic (p110) sub-unit. A simple model for activation by growth factors has been proposed ([14]): PI3K complexes are recruited to the plasma membrane through the interaction between the SH2-domains in their regulatory subunits and the phospho-tyrosine residues on the receptor. There, the catalytic sub-unit of PI3K is stabilized and comes in close proximity with phosphoinositides. PI3K phosphorylates phosphoinositides on the D3 position of their inositol ring. This generates the second messengers phosphatidylinositol-3,4-biphosphate (PI-3,4-P_2) and phosphatidylinositol-3,4,5-triphosphate (PIP_3) from the respective substrates (PI-4-P and PI-4,5-P_2) ([14]).

In the AKT-pathway the relevant process is the PI3K-mediated conversion of PIP_2 to PIP_3 ([42]). The PH-domain of AKT binds to PIP_3 leading to increased recruitment of AKT to the cell membrane (see figure 2.2).

ZSTK474 [2-(2-difluoromethylbenzimidazol-1-yl)-4,6-dimorpholino-1,3,5-triazine] is a s-triazine derivative that strongly inhibits the growth of tumor cells ([44]). It is suggested that ZSTK474 binds to the ATP-binding site of PI3K ([44]), thereby inhibiting the conversion of PIP_2 to PIP_3. ZSTK474 was used in the experiments for this thesis as a pathway inhibitor.

FoxO1 and Protein Kinase B: PKB/AKT

Protein kinase B is usually either abbreviated to *PKB* or the term *AKT* is used. The existence of two names is due to its initial identification by

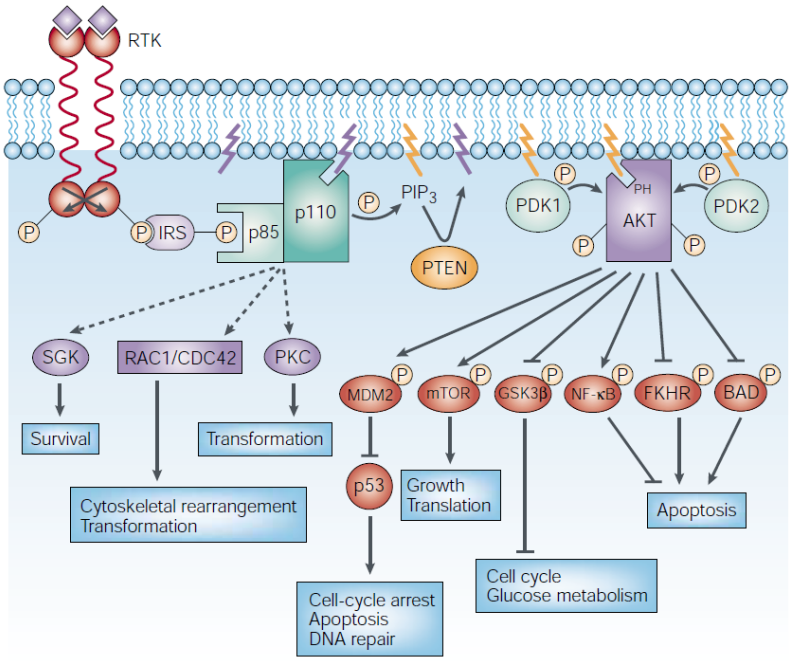

Figure 2.2: AKT-activation through PI3K-mediated conversion of PIP_2 to PIP_3. The p85-subunit of PI3K binds to IRS1 and the p110-subunit catalyzes the conversion of the phosphoinositides. Additionally, some of the cellular targets of both AKT and PI3K (dashed lines, as they are yet poorly characterized) are shown. (Figure from [42]).

three independent groups ([38]). Two groups named it after its homology to protein kinases A and C, while one group derived a name from AKT being the cellular homolog to retroviral oncogene "viral-akt". The origin of this term dates back to as far as 1928 and is merely a result of numbering mouse cultures. AKT is a protein kinase that phosphorylates proteins at serine or threonine amino-acid side chains. AKT is therefore a member of a family of proteins called Serine/threonine-specific protein kinases (STK). It is a very versatile and important protein kinase at the core of human physiology and disease ([30]).

In mammals, three forms of AKT have been identified: AKT1, AKT2 and AKT3. They feature the same characteristic domain structure: An amino-terminal PH-domain, a central kinase domain and a carboxyl-terminal regulatory domain ([38]). The PH-domain is named after Pleckstrin, the protein in which it was first discovered and it serves to bind to phosphoinositides (such as PIP_3) with high affinity.

PIP_3 plays a dual role in AKT activation: it recruits AKT to the membrane and activates 3-phosphoinositide-dependent protein kinase 1 (PDK1) ([2]). PDK1 and PDK2 phosphorylate AKT at Thr308 and Ser473, causing full activation of AKT ([42]).

PI3K-dependent AKT activation is counterbalanced by the tumor suppressor PTEN, which converts PIP_3 to PIP_2 ([41], [40]). PTEN is mutated in many forms of human cancer ([36]). Mutations in PTEN result in increased PIP_3 levels, which trigger constitutive AKT activation and uncontrolled proliferation ([24]).

AKT activation can be measured by monitoring the translocation to the cytoplasm of its direct target FoxO1a, a member of the Forkhead family of transcription factors involved in cell cycle progression ([20]).

mTOR and rapamycin

Rapamycin is an antifungal metabolite produced by a bacterial strain called *Streptomyces hygroscopius* which was discovered in a soil sample from the Easter Islands ([9]). It was named after the native word for the Easter Islands: *Rapa Nui*. Soon after its discovery, Rapamycin (also called *sirolimus*) was found to exhibit immunosuppressive effects and suppress cell proliferation ([9]). Research subsequently focused on finding the target protein of rapamycin, which was identified in yeast and named TOR (Target of Rapamycine).

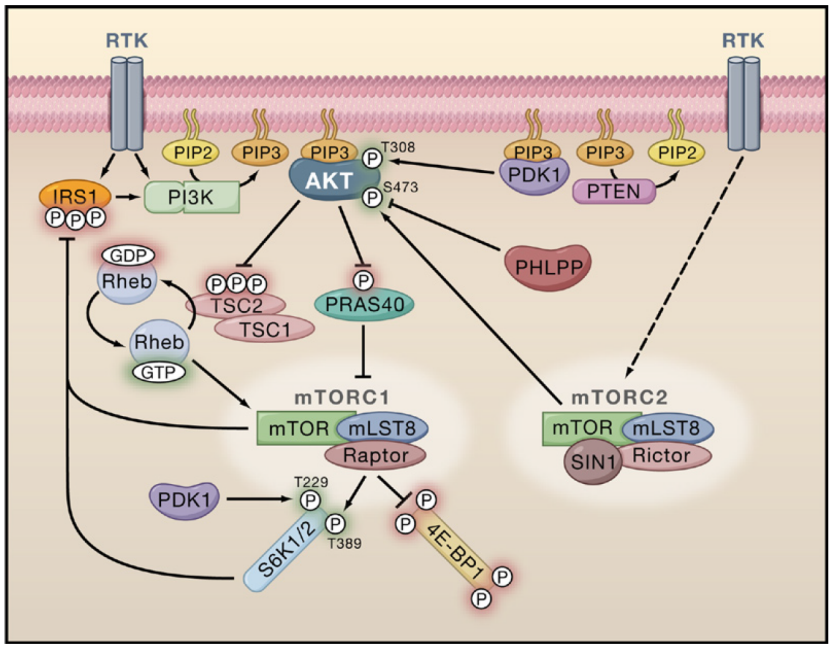

Figure 2.3: The role of the two mTOR-complexes in the AKT pathway. Note the negative feedback loop consisting of IRS1, AKT and mTORC1 (Figure from [30]).

Target of Rapamycin (TOR) is an evolutionarily conserved Serine/Threonine protein kinase. It is found in yeast, worms, flies and mammals ([13]). While yeast contains two distinct TOR genes to form two distinct Tor-complexes (Tor1 to form Tor-Complex-1 and Tor2 to form Tor-Complex-2), higher eukaryotes contain only one TOR gene (e.g. mTOR = *mammalian* TOR, dTOR, ceTOR) to form both complexes.

TOR-complex 1 (TORC1) and TOR-complex 2 (TORC2) are functionally distinct complexes that share their catalytic core (which is mTOR in mammals) and a few of their other partner proteins ([13]). However, since they do not share *all* of their partner proteins, their behavior is quite different. Both complexes and their role in the AKT-pathway are shown in figure 2.3. The defining subunit of mTORC1 is the Rapamycin-sensitive adaptor protein of mTOR, called *Raptor* and the defining subunit of mTORC2 is the Rapamycin-insensitive companion of mTOR, called *Rictor*.

For the presented thesis, one more interaction was of central importance: mTORC1 (via an intermediate step employing S6K1) phosphorylates IRS1 at the plasma membrane and thereby *suppresses* the activation of AKT via

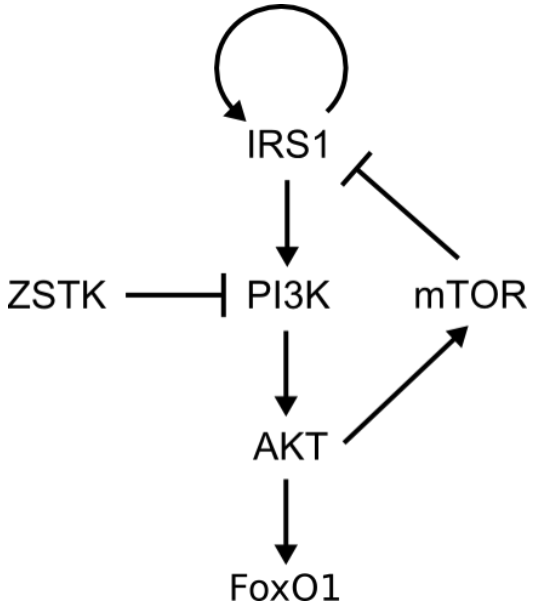

Figure 2.4: A schematic overview of the AKT pathway. ZSTK, being a synthetic drug, is not present naturally.

PI3K ([4]). This constitutes a negative feedback loop. Rapamycin inhibits mTORC1 and attenuates that negative feedback loop ([4]).

2.2.2 Functional pathway scheme

As described in the chapter above, IRS-1 recruits PI3K to the membrane and thereby activates it. PI3K turns PIP_2 into PIP_3, which recruits PDK1, PDK2 and AKT to the membrane. PDK1 and PDK2 phosphorylate AKT. Among other targets, AKT also indirectly activates the mTOR-complex-1. This complex deactivates IRS-1, constituting a negative feedback loop. Furthermore, AKT directly phosphorylates IRS1 at Ser629, preventing an inhibitory phosphorylation at Ser636 ([29]). Because IRS1 is upstream of AKT, this defines a positive feedback loop. Omitting the PIP/PDK-step and adding ZSTK and FoxO1 as the input-/output-variables used in the experiments, the pathway can be sketched as in figure 2.4.

2.3 How to observe pathway activities: Immunofluorescence

2.3.1 General remarks

Since the very beginning of cell biology, optical microscopy has played a key role in the advancement of the field. A typical animal cell is $10 - 20\,\mu m$ in diameter ([1]) and mostly colorless and translucent. Historically, the invention and discovery of stains (late 19th century) and methods such as the phase-contrast microscope, the dark-field microscope or the differential-interference-contrast microscope were important milestones.

It is important to emphasize that microscopy of biomolecules crucially depends on both the microscope *and* the preparation of the specimen.

2.3.2 Fluorescence microscopy

The fluorescence microscope itself is very similar to an ordinary light microscope. The crucial addition to the beam path are two wavelength filters and a beam-splitting, dichroic mirror (see figure 2.5). Typically, these 3 parts are combined to form a "filter cube". The first filter only transmits light within a narrow range of wavelengths (the *excitation wavelength*). The beam-splitting mirror then reflects this beam of light onto the sample. The fluorescent molecules in the sample then absorb the excitation light and (after a short delay) emit light at a different wavelength (the *emission wavelength*). Due to energy conversion losses, the emission wavelength is always higher than the excitation wavelength. The emitted light can pass the beam-splitting mirror and the second filter, which blocks any remaining excitation or ambient light. Finally, light arrives at the detector, which may typically be the eye or a CCD camera.

Widely used fluorescent dyes are fluorescein (FITC), rhodamine and the more modern Cy3, Cy5 and the Alexa dyes. Using multiple dyes with different absorption/emission spectra allows for simultaneous detection of different molecules.

A powerful method to achieve this coupling of target molecules to fluorescent molecules is the binding of the fluorescent dye to antibodies that are specific to the molecule of interest. This approach is known as *Immunofluorescence* and will now be discussed in more detail since it was the method of choice for this thesis.

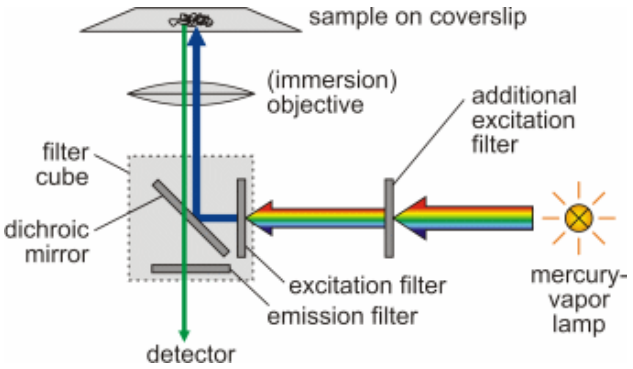

Figure 2.5: Principle of a fluorescence microscope. More specifically, an inverted setup with a mercury-vapor lamp as the light source is shown. (Figure taken from diploma thesis of Steve Pawlizak, 2009, University of Leipzig)

2.3.3 Immunofluorescence

Antibodies (ABs) are proteins that are a main part of the vertebrate immune system. They exist in billions of different forms ([1]) to recognize and bind to specific target molecules (*antigens*). The precision offered by this specificity makes antibodies valuable probes for fluorescence microscopy approaches. To amplify the signal, a highly specific, but unmarked *primary AB* is bound to the target molecule. Subsequently, a *secondary AB* (which carries the fluorophore) binds to the primary AB. This method is called *indirect immunofluorescence* as opposed to *direct immunofluorescence* in which the primary ABs carry the fluorophore.

Problems and limitations of immunofluorescent approaches include ([35]):

- Photobleaching: The destruction of the fluorophore due to the generation of reactive oxygen species as a byproduct of fluorescence excitation. Photobleaching can be minimized by reducing the intensity and duration of the excitation light or the addition of antifade reagents (that reduce the availability of singlet oxygen).

- Autofluorescence: In mammalian cells, flavin coenzymes (FAD and FMN) and reduced pyridine nucleotides (NADH) fluoresce on their own. This can be minimized by appropriate selection of filters.

- Fluorescence Overlap: When measuring fluorescence signals of more than one color, it is possible that the emission spectra of the used dyes overlap. This might lead to an overestimation of the measured signal

in one color and should be avoided by choosing appropriate dyes and filters.

Depending on the molecule of interest and the investigated cell type or tissue, a number of preparatory steps is required. These may include sectioning, freezing, disrupting cell membranes (permeabilization), etc. The protocols used during the experiments within this thesis are given in 8.

Chapter 3

Mathematical Theory

3.1 Introduction to Modeling

This chapter is aimed at giving the reader a brief introduction to mathematical modeling as it is employed in biology. The presentation mainly follows the Books "Mathematical Biology" by J. D. Murray ([34]), "Non-Linear-Dynamics and Chaos" by Strogatz ([39]) and "Mathematical Physiology" by Keener and Sneyd ([21]).

The examples given shall aid the reader to gain some intuition of what behavior can be expected from a system with certain features (such as feedback, non-linearities). Furthermore, this section is used to define important terms such as *Stability*, *Steady State* and analysis tools like the *rate balance plot* and the *dose-response curve*.

3.1.1 Models for Single Species

Probably the oldest subject of mathematical modeling has been the study of population dynamics. Its history goes back as far as 1202 ([34]) and has since been applicated in a vast number of fields.

The basic assumption is the following: Let $N(t)$ be the population of a species at a time t. Then

$$\frac{dN}{dt} = births - deaths \tag{3.1}$$

is the rate of change of the population (assuming that change only arises from birth and death of individuals). In the simplest model, births and deaths are proportional to the population number N: $births = k_1 N$, $deaths = k_2 N$

(with k_1 and k_2 being positive constants) resulting in

$$\frac{dN}{dt} = k_1 N - k_2 N \tag{3.2}$$

which gives, after integration

$$N(t) = N_0 e^{(k_1 - k_2)t} \tag{3.3}$$

For $k_1 > k_2$ the population grows (see figure 3.1), for $k_1 < k_2$ the population decays. Introducing $r = k_1 - k_2$, equation (3.3) becomes

$$N(t) = N_0 e^{rt} \tag{3.4}$$

In physics, this equation is especially well known for $r < 0$ as it accurately describes e.g. the decay of radioactive substances or the attenuation of light intensity propagating in an absorbing medium (with time t being replaced by penetration depth).

In biological systems, the assumptions of linear dependence of birth- and death-rates on the current size of population are often far too much simplified.

A biologically plausible way to account for limited resources (space, food) is to include a carrying capacity K in the model. The carrying capacity is then defined as the number of individuals which prevents further increase (so for $N = K$, $\frac{dN}{dt} = 0$ shall be valid). This can mathematically be achieved by multiplying (3.2) by $(1 - \frac{N}{K})$, yielding

$$\frac{dN}{dt} = rN(1 - \frac{N}{K}) \tag{3.5}$$

with r defined as before.

Integration gives the *logistic growth law*

$$N(t) = \frac{N_0 * K * e^{rt}}{K + N_0(e^{rt} - 1)} \tag{3.6}$$

which is plotted in figure 3.2.

Note that the same behavior is observed when modeling the reaction $A + N \rightarrow N + N$ using the law of mass action (see chapter 3.2.1).

3.1.2 Models for Interacting Species

Things become more complicated when we take into consideration that ecosystems never consist of only one species. Two species can interact competitively (both species hinder each other), they can mutually benefit

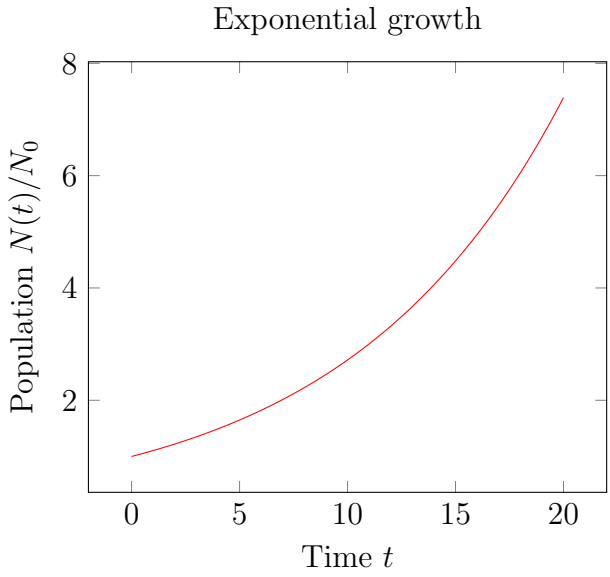

Figure 3.1: Exponential growth as described by 3.3 for $r = 0.1$

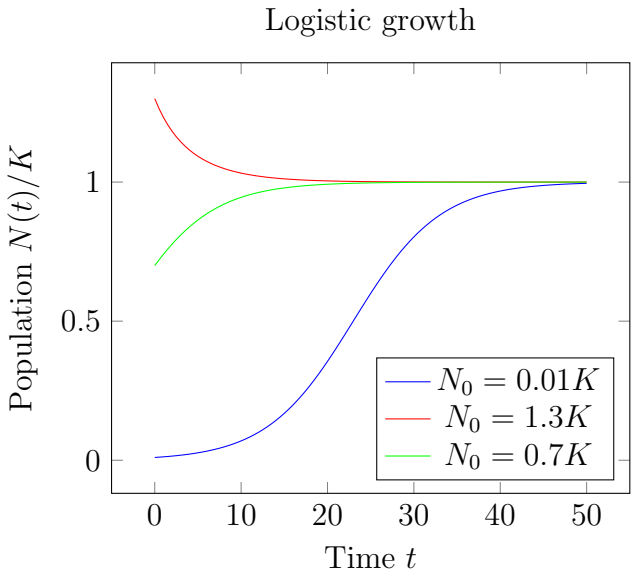

Figure 3.2: Logistic growth as described by 3.6 for $r = 0.2$

from each other (symbiosis) or one species eats the other. The last case is discussed in the classic "predator-prey"-model. The model dates back to the 1920s and is named after both *Alfred J. Lotka* and *Vito Volterra*. Lotka derived the equations from a *hypothetical* chemical reaction that could exhibit oscillations while Volterra proposed the model to explain the oscillatory levels of certain fish catches ([34]).

The assumptions of the model are: There are two species, "prey" N and "predator" P. Without each other, the prey is allowed to grow indefinitely while the predator is going extinct, following eq. 3.4 with $r > 0$ for the prey and $r < 0$ for the predator.

The interaction of the two now limits the behavior by adding a decay-term for the prey and a growth-term for the predator. Both terms are proportional to *both* species, yielding

$$\frac{dN}{dt} = aN - bPN \tag{3.7}$$

$$\frac{dP}{dt} = cNP - dP \tag{3.8}$$

In this representation, a, b, c and d are all positive.

A standard tool for analyzing systems like this is *non-dimensionalization*. Non-dimensionalization reveals how many parameters are actually *necessary* to determine the behavior of the system. For the Lotka-Volterra-model, we can define $n = \frac{cN}{d}$, $p = \frac{bP}{a}$, $\tau = at$ and $\alpha = d/a$ to re-write equations 3.7, 3.8 as

$$\frac{dn}{d\tau} = n(1 - p) \tag{3.9}$$

$$\frac{dp}{d\tau} = \alpha p(n - 1) \tag{3.10}$$

It is possible to plot parametrical solutions of this system in the n, p plane, that is, without representing time. Eliminating time from the above system yields:

$$\frac{dn}{d\tau} = \alpha \frac{p(n-1)}{n(1-p)} \tag{3.11}$$

Integrating 3.11 gives the phase trajectories

$$\alpha n + p - \ln n^{\alpha} p = H \tag{3.12}$$

with $H > H_{min} = 1 + \alpha$ being a positive constant. Figure 3.3 shows some of the trajectories. Note that the trajectories are closed, indicating periodic solutions.

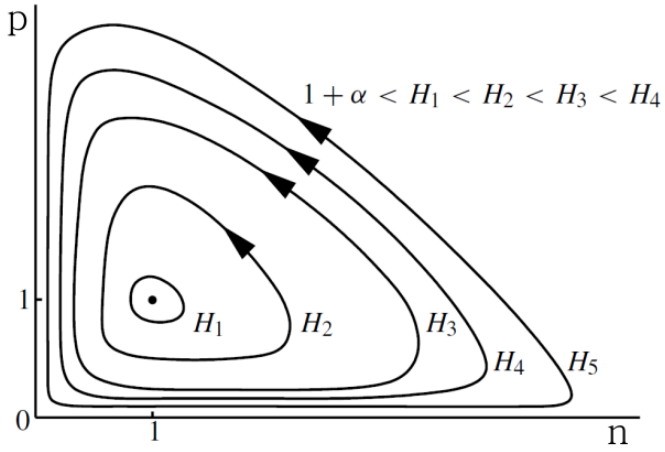

Figure 3.3: Phase-Plane trajectories for various values of H for the Lotka-Volterra system. The arrows denote the direction of change with increasing time τ. (Figure adapted from [34])

3.2 Reaction Kinetics

This chapter is based on the book by Keener and Sneyd ([21], sections 3.2.1, 3.2.2), the original papers by Goldbeter and Koshland ([16],[23], section 3.2.3) and the paper by Ferrell ([12], section 3.3).

3.2.1 The law of mass-action

In modeling cellular networks, complexity does not arise from the necessary equations themselves, but from the complexity of the networks.

The basic equations are all rather simple. The most basic reaction $A+B \rightarrow C$ can be modeled using the *law of mass action*:

$$\frac{d[C]}{dt} = k[A][B] \tag{3.13}$$

$\frac{dC}{dt}$ is the accumulation of the product C, while $[A]$ and $[B]$ give the concentrations of the educts A and B, respectively. The *reaction constant* k incorporates all other properties of the reaction, such as size and shape of the educts, temperature, et cetera.

The law of mass action is not sufficient to accurately model very low concentrations, concentrations at which the reaction saturates or changing temperatures. Furthermore, due to thermodynamics, we have to take into

consideration that the backward reaction $C \rightarrow A + B$ is also possible. The more complete reaction scheme should therefore be written as:

$$A + B \underset{\mathrm{k_2}}{\overset{\mathrm{k_1}}{\rightleftarrows}} C \tag{3.14}$$

Applying the law of mass action gives the following rate law:

$$\frac{d[C]}{dt} = k_1[A][B] - k_2[C] \tag{3.15}$$

To model reactions of the type $A + A \overset{\mathrm{k_1}}{\underset{\mathrm{k_2}}{\rightleftarrows}} C$, one must take into consideration the stochastic weights of the molecule species:

$$\frac{d[C]}{dt} = \frac{1}{2}k_1[A]^2 - k_2[C] \tag{3.16}$$

3.2.2 Michaelis-Menten Kinetics

Enzymes are biological catalysts. They can increase the rate of a catalyzed reaction by a factor of 10^{12} or more. Many cellular processes are possible only because each cell is equipped with its own set of enzymes. Therefore, enzyme-catalyzed reactions play a crucial role in biological systems. (adapted from: [22])

Enzymatic reactions can be written as a substrate S, forming a product P, when combined with an enzyme E:

$$S + E \underset{\mathrm{k_{-1}}}{\overset{\mathrm{k_1}}{\rightleftarrows}} P + E \tag{3.17}$$

Experiments show, that enzyme kinetics usually do not follow the simple mass-action law described above. Typically, increasing the amount of substrate only increases the reaction rate until a level of saturation is reached (whereas the law of mass action predicts a linear dependence of the reaction rate on the substrate concentration).

A widely used model was proposed by Michaelis and Menten in 1913. The model introduces a transition state C (for complex). The substrate forms a complex with the enzyme and the complex can then break down into the product (and the enzyme). The scheme then looks like this:

$$S + E \underset{\mathrm{k_{-1}}}{\overset{\mathrm{k_1}}{\rightleftarrows}} C \underset{\mathrm{k_{-2}}}{\overset{\mathrm{k_2}}{\rightleftarrows}} P + E \tag{3.18}$$

In many cases, it is justified to further simplify the scheme by neglecting the back-reaction of the final product (for instance, if the final product is constantly removed).

$$S + E \underset{\mathrm{k}_{-1}}{\overset{\mathrm{k}_1}{\rightleftarrows}} C \xrightarrow{k_2} P + E \tag{3.19}$$

Applying mass-action rate laws to this reaction scheme yields the following set of differential equations:

$$\frac{d[S]}{dt} = k_{-1}[C] - k_1[S][E] \tag{3.20}$$

$$\frac{d[E]}{dt} = (k_2 + k_{-1})[C] - k_1[S][E] \tag{3.21}$$

$$\frac{d[C]}{dt} = k_1[S][E] - (k_2 + k_{-1})[C] \tag{3.22}$$

$$\frac{d[P]}{dt} = k_2[C] \tag{3.23}$$

Since $\frac{d[E]}{dt} = -\frac{d[C]}{dt}$, it follows that the quantity $[C] + [E] = E_0 = const.$ is conserved. Note that $[P]$ can be calculated by direct integration.

There are two famous approximations for the Michaelis-Menten model:

- The Equilibrium Approximation
- The Quasi-Steady-State Approximation

The equilibrium approximation was the original approximation proposed by Michaelis and Menten in 1913, while the quasi-steady-state approximation was proposed by Briggs and Haldane in 1925.

The basic assumption of the equilibrium approximation is that the substrate is in immediate equilibrium with the complex, $k_1[S][E] = k_{-1}[C]$. This is equivalent to asking that the process $C \xrightarrow{k_2} P + E$ be much slower than the first step. The second (the slower) process is then referred to as the *rate-limiting process*.

In the quasi-steady-state approximation, it is assumed that the rate of complex-formation and breakdown are approximately equal (so $\frac{d[C]}{dt} \approx 0$). A more thorough mathematical analysis (employing non-dimensionalization) translates this assumption to the requirement that $\frac{E_0}{S_0} \ll 1$, typically in the

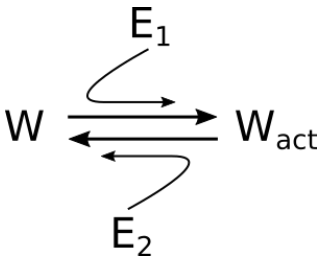

Figure 3.4: The reaction scheme modeled by Goldbeter and Koshland. If, for instance, W_{act} were to be the phosphorylated form of a protein W, the enzyme E_1 would be a kinase and E_2 a phosphatase.

range of 10^{-2} to 10^{-7}. This is a reasonable assumption in enzymatically catalyzed reactions in biological systems.

The results of the two approximations look rather similar, leading sometimes to confusion. In both cases, the result takes the form:

$$\frac{d[P]}{dt} = \frac{k_2 E_0[S]}{[S] + K_{MM}} \tag{3.24}$$

The difference lies in the definition of K_{MM} and the assumptions of the models. In the equilibrium approximation,

$$K_{MM} = \frac{k_{-1}}{k1} \tag{3.25}$$

while in the *quasi-steady-state approximation*,

$$K_{MM} = \frac{k_{-1} + k_2}{k1} \tag{3.26}$$

For a more detailed discussion and derivation of the two approximations, the book *Mathematical Physiology* ([21]) is recommended.

3.2.3 The Goldbeter-Koshland model

In 1982, Goldbeter and Koshland proposed an elegant mechanism to model highly sensitive switching behavior. Unlike other models, they do not rely on high Hill-coefficients caused by highly cooperative processes such as multiple enzyme-binding sites, cooperativity between many enzymes or the like.

The Goldbeter-Koshland model can be sketched as in figure (3.4). A substrate W can exist in one of two forms, W and W_{act}, for instance. The

reaction $W \to W_{act}$ is catalyzed by an enzyme E_1 and the reaction $W_{act} \to W$ is catalyzed by E_2. This produces the system:

$$W + E_1 \underset{\mathrm{k}_{-1}}{\overset{\mathrm{k}_1}{\rightleftarrows}} C_1 \xrightarrow{k_2} E_1 + W_{act} \tag{3.27}$$

$$W_{act} + E_2 \underset{\mathrm{k}_{-3}}{\overset{\mathrm{k}_3}{\rightleftarrows}} C_2 \xrightarrow{k_4} E_2 + W \tag{3.28}$$

It is then possible to model both reactions with Michaelis-Menten approximations.

$$\frac{d[W_{act}]}{dt} = \frac{k_2 E_1[W]}{[W] + K_1} - \frac{k_4 E_2[W_{act}]}{[W_{act}] + K_2} \tag{3.29}$$

$$\frac{d[W]}{dt} = -\frac{d[W_{act}]}{dt} = \frac{k_4 E_2[W_{act}]}{[W_{act}] + K_2} - \frac{k_2 E_1[W]}{[W] + K_1} \tag{3.30}$$

In a steady state, $\frac{d[W]}{dt} = 0$, it follows from 3.30 that

$$\frac{k_2 E_1[W]}{[W] + K_1} = \frac{k_4 E_2[W_{act}]}{[W_{act}] + K_2} \tag{3.31}$$

which can be written as

$$\frac{k_2 E_1}{k_4 E_2} = \frac{[W_{act}]([W] + K_1)}{([W_{act}] + K_2)[W]} \tag{3.32}$$

Substituting $\frac{v_1}{v_2} = \frac{[E_1]k_2}{[E_2]k_4}$ and normalizing $y = \frac{[W]}{[W_{act}]+[W]}$ and $\hat{K}_i = K_i/W_{tot}$ gives

$$\frac{v_1}{v_2} = \frac{(1-y)(\hat{K}_1 + y)}{y(\hat{K}_2 + 1 - y)} \tag{3.33}$$

The dependence of y (which is the ratio $\frac{W}{W_{tot}}$ with $W_{tot} = W + W_{act}$) on the ratio $\frac{v_1}{v_2}$ is shown in figure 3.5. It can be seen that the Goldbeter-Koshland-function produces highly sensitive, non-linear behavior. The ratio $\frac{v_1}{v_2} = \frac{[E_1]k_2}{[E_2]k_4}$ can be influenced by either varying the reaction coefficients or the amount of enzyme. The function thereby offers a way to model switches in reaction networks.

3.3 Steady States and Rate-Balance plots

Bistability provides a mechanism to create irreversibility in cell life cycles and cell signaling. This is not a trivial property, since the basic biochemical

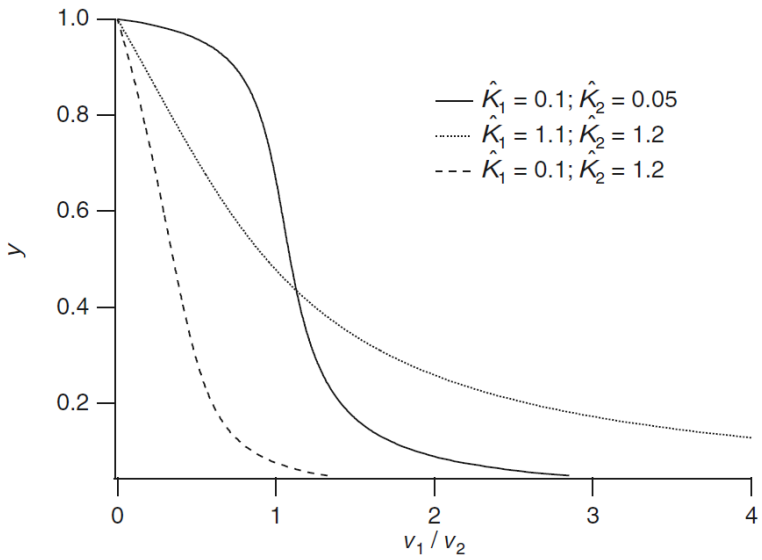

Figure 3.5: Plots of $y = [W]/[W_{tot}]$ as a function of v_1/v_2 for different values of K_i. Note the step-like behavior for low values of K_i. (Figure from [21])

reactions involved are all reversible ([11]) (Proteins are phosphorylated and dephosphorylated, degraded and synthesized etc.).

As early as in 1961, it was proposed that one possible mechanism for creating irreversibility (or memory) is in the way the pathways are wired (see [33]). In perfect analogy to electrical engineering, we try to work our way up from simple basic circuits or circuit elements to complex signaling networks.

From today's understanding, bistability in biological systems relies on a feedback loop (either positive, double-negative or autocatalysis) and some type of non-linearity ([11]).

To understand this, it is helpful to become acquainted with *rate-balance plots*. These are a major tool in chaos theory and are explained thoroughly in Strogatz' book "Non-Linear Dynamics and Chaos" ([39]).

The concept is the following: If the change of a quantity is given by a rate law in the form $\frac{dN}{dt} = f(N, p_i)$, then any state where $\frac{dN}{dt} = 0$ is called a *steady state*. If the function $f(N, p_i)$ can be split into two separate parts $f(N) = f_{prod}(N, p_i) - f_{dec}(N, p_i)$, the zero points of $f(N)$ become the intersections of $f_{prod}(N, p_i)$ and $f_{dec}(N, p_i)$. This means that the number of steady states can be found by counting the number of intersections, as demonstrated in figure 3.6.

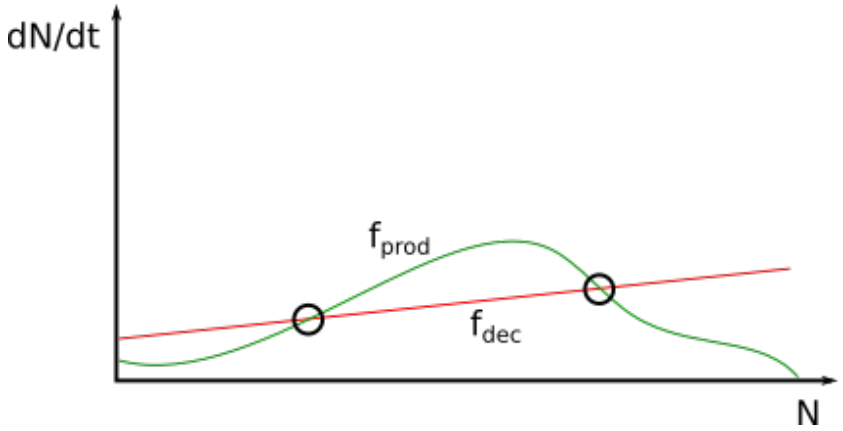

Figure 3.6: A hypothetical rate-balance plot. The intersections of f_{prod} and f_{dec} are steady states of the system. It can immediately be seen that the system has two steady states (marked with circles).

The separation of $f(N, p_i)$ can contain biological meaning: $f_{prod}(N, p_i)$ and $f_{dec}(N, p_i)$ can group reactions that produce and break up the substance N, respectively.

As an additional benefit, the graphic representation makes it easy to distinguish between *stable* and *instable* steady states:

So far, we have defined that N_{steady} is a steady state when $f_{prod}(N_{steady}) = f_{dec}(N_{steady})$.

We now declare N_{steady} to be a *stable* steady state when $f_{prod}(N) > f_{dec}(N)$ for $N < N_{steady}$ and $f_{prod}(N) < f_{dec}(N)$ for $N > N_{steady}$. This is equivalent to asking for $\frac{d^2N}{dt^2}(N_{steady}) < 0$. However, the first formulation can easily be applied to analyze rate-balance-plots, as demonstrated in figure 3.7. This helps greatly in understanding the influence of parameters on the qualitative behavior of a complex system.

3.3.1 Bistability and Hysteresis

Employing the tools from the above section, we shall now analyze how a system can exhibit bistability. A system is called *bistable* when there are two *stable* steady states. For continuous functions $f(N, p_i)$, this implies the existence of a third, unstable steady state in between (see figure 3.8). The unstable steady state is also referred to as the threshold, as it marks the amount of N needed for the system to continue towards the high state.

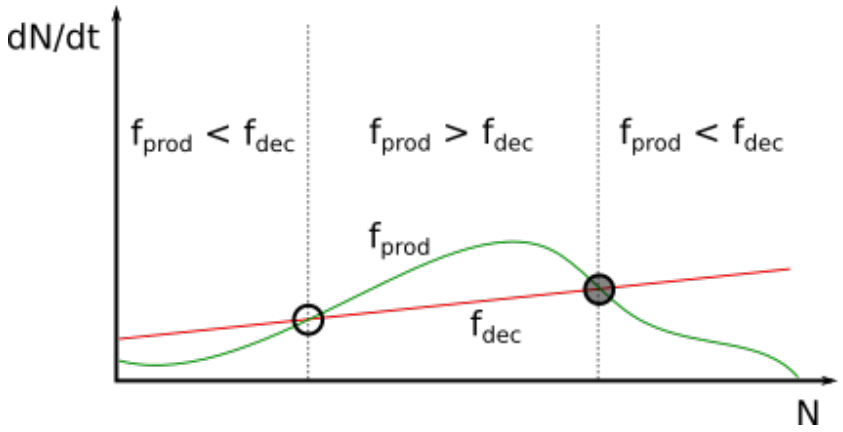

Figure 3.7: The same hypothetical rate-balance plot as in figure 3.6. It can be seen that only the high steady state is stable: A small decrease of N results in net production of N, therefore increasing N again. In case N increases beyond N_{steady}, a net decay reduces N back to N_{steady}.

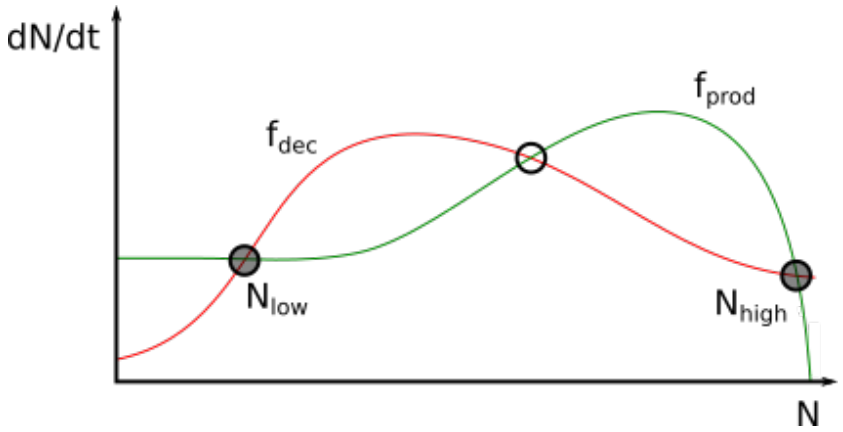

Figure 3.8: A rate-balance plot with two stable steady states (dark circles) and one threshold unstable state in between (light circle).

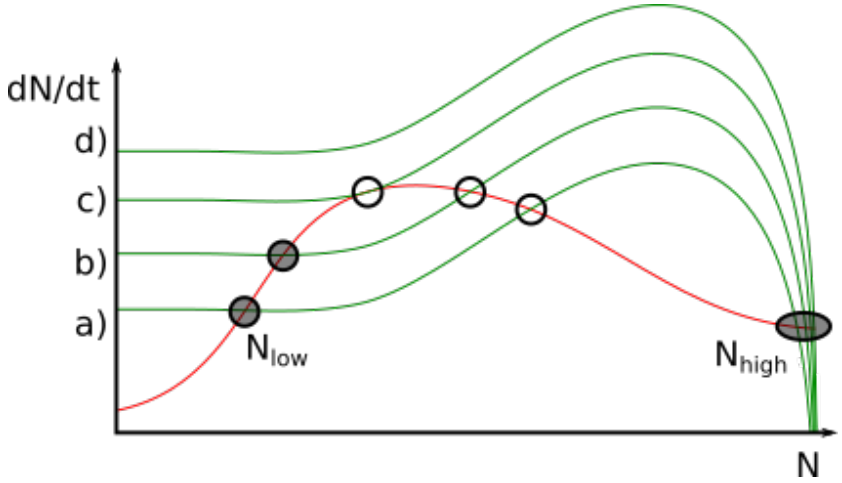

Figure 3.9: Suppose a stimulus can be applied to the system that increases the production rate by a constant amount. In the figure, 4 exemplary stages are shown then: a) the original case with two stable states, b) a little stimulus only shifts the states but does not change their number, c) more stimulus removes the low steady state, d) only the high steady state remains.

The remaining question is, which biological phenomena can plausibly be modeled by such rate-balance plots? An important paper by James E. Ferrell from 2001 ([12]) lists two mechanisms that can lead to bistability in biological systems:

- Nonlinear positive feedback
- Back reaction saturation

Bistable systems can function as biological switches, in many case as irreversible ones. This can be understood by considering figure 3.9. Suppose the system rests in the (stable) state N_{low}. If some stimulus increases the forward reaction rate, all the steady states are shifted. If at some point, the system becomes monostable, the system will naturally reach that single steady state, which is N_{high} in the example. After removing the stimulus (resetting the rates), the system will remain in the high state.

The above system exhibits *Hysteresis*, as its state does not only depend on the current parameters, but also on its history.

The situation can also be plotted in another way, as the realized state of the system depending on the current input stimulus. This is shown in figure 3.10.

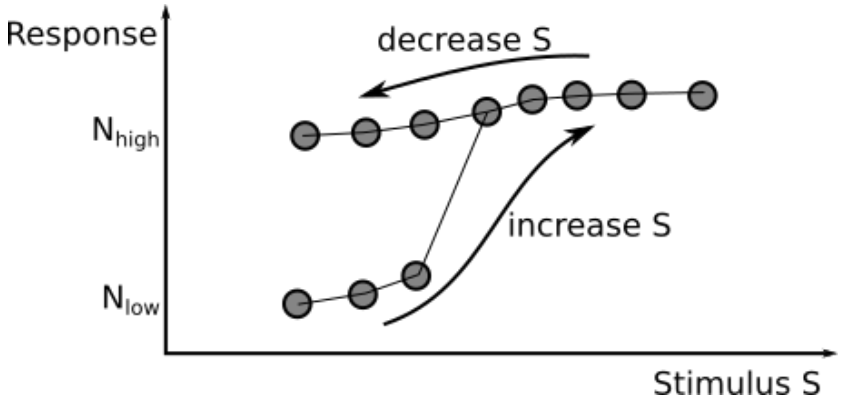

Figure 3.10: A hysteretic Dose-Response Curve. Increasing the stimulus S above a certain threshold abruptly changes the state of the system. The system remains in that state even when the stimulus is again reduced.

This constitutes the case of an *irreversible* switch. The more general case (though sometimes harder to realize) is the reversible switch, illustrated by figure 3.11. In this case, the system reaches its original state when the stimulus is completely removed.

In general, hysteresis occurs in a system, when there is a parameter range where multiple steady states are possible for the same input values. The simplest possibility being two stable steady states within the range and just one stable steady state for the parameter being outside the range. The system then remains in the steady state that was achieved before the parameter entered the range of multiple stabilities.

3.3.2 Proteresis

An easily overlooked phenomenon is inverted hysteresis, sometimes called "clockwise" hysteresis. For reasons explained further below, the terms "clockwise" and "counter-clockwise" are quite ambiguous, so the term "Proteresis" was coined to emphasize that it is actually a phenomenon distinct from Hysteresis. Clockwise hysteresis loops are quite common in pharmacodynamics (e.g. [28]). However, in pharmacodynamics they result from plotting Dose-Response curves over time and the resulting hysteresis can easily be explained by delay-effects in the human organism. In physics, real proteresis was recently observed in the magnetism of ultrasmall Co:CoO core-shell nanoclusters (see [43] and [25]). Furthermore, a proteretic all-optical bi-stable device was theoretically designed and modeled for possible use in the field of Optics Communications ([8]).

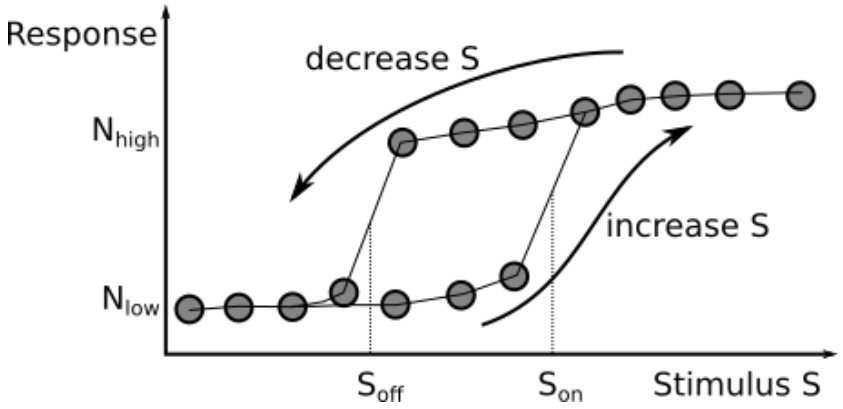

Figure 3.11: A general, hysteretic dose-response curve. For a certain range of stimulus intensity (between S_{off} and S_{on}), the state of the system depends on its history.

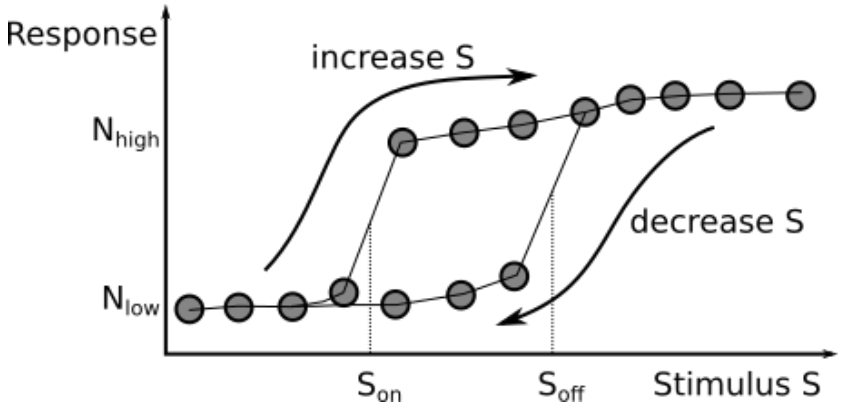

Figure 3.12: An inverted hysteresis or "proteresis" curve. Comparing the figure to fig. 3.11 shows that $S_{on} < S_{off}$

The interesting property of proteretic loops is their "anticipatory" behavior. A proteretic switch can be turned on at a threshold S_{on} and turned off at a threshold S_{off} with $S_{off} > S_{on}$. For a hysteretic switch, $S_{off} < S_{on}$ is the case. Which state the system will be in when S is between S_{on} and S_{off} depends on the history of the system for both cases.

A hysteretic system will be in the low state if it was in the low state before and in the high state, if it was in the high state before. This behavior has a very "natural" or "conservative" feeling to it. A proteretic system will be in the high state if it was in the low state before and in the low state if it was in the high state. This is obviously more exotic as it constitutes a bistable device that has two stable states, but is easier to switch from one state to

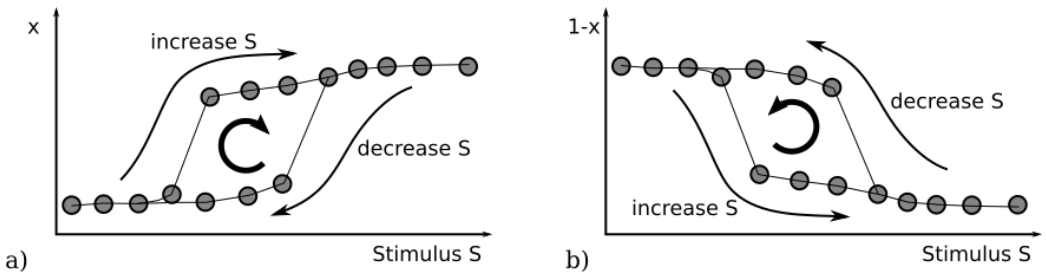

Figure 3.13: a) The same, proteretic system as in figure 3.12. b) The same system, but instead of x, $(1 - x)$ is the observable quantity. The system's behavior now appears counter-clockwise.

the other than to keep in its original state.

In literature, proteresis is often described as "clock-wise hysteresis". However, when observing a quantity that decreases when the input is increased, the connections counter-clockwise $\leftrightarrow$ hysteresis, clock-wise $\leftrightarrow$ proteresis do not hold. In the simplest case, we might measure $(1 - x)$ instead of x. Figure 3.13 illustrates the problem: Measuring $(1 - x)$ instead of x flips the dose-response curve upside-down. And even though this curve still describes the same system, it is no longer "clock-wise" but "counter-clockwise".

Especially in biology, it is very likely that only one form of e.g. an enzyme can be observed (e.g. only the phosphorylated form), leading to dose-response curves that can be clockwise or not. To decide whether a system is proteretic or hysteretic, the defining characteristic is whether it *keeps* or *changes* its state when entering the bistable region.

Chapter 4

Materials and Methods

Fluorescence microscopy is a standard method in cell biology today. However, applying the general method to a specific cell type and a specific target molecule still provides a challenge. In the presented thesis, it proved to be difficult finding suitable antibodies and a working staining protocol.

Mathematical modeling of cellular signaling pathways is still a comparatively young field of study. At the moment, a lot of effort is put into classifying general motifs or "building blocks" of pathways in order to understand, what interactions are necessary and which are sufficient to generate certain behaviors. A good example are the works of J. E. Ferrell ([10],[12],[11]), A. Carracedo and P. Pandolfi ([6],[5]) or D. A. Charlebois ([7]) who try to identify feedforward motifs, feedback loops and analyze what implications those have on drug development.

The general method involves writing down a system of differential equations to model the biological system. To analyze that system, analytical tools like phase-plane-analysis or bifurcation diagrams (explained in chapter 3) can be used. For bigger systems, these methods fail. It is then necessary to either

1. Simplify the system

2. Analyze the system numerically

or a combination of the two. Simplifying the system to a degree where analytical methods become feasible might make the biological system unrealistic and/or prevent the mathematical system from exhibiting the desired (observed) behavior. For these reasons, numerical analysis is becoming more important and widely-used.

4.1 Numerical Methods

As mentioned, in the field of systems biology, analytical tools are mainly used to study smaller parts of pathways. To model more complex pathways (or even "complete" pathways), numerical methods are necessary.

Models of cellular signaling pathways are typically made from rate-law equations. As a result, the pathway is modeled as a system of first-order ordinary differential equations (ODEs).

The *Runge-Kutta-method* is a popular way to approximate numerical "solutions" for such systems. The classic Runge-Kutta-method is defined as follows (from [17]):

For the equation $y'(x) = f(x, y)$ with initial condition $y(x_0) = y_0$, a solution $y(x)$ can be approximated through recursive use of:

$$y(x_{i+1}) = y(x_i) + \frac{1}{6}h(k_1 + 2k_2 + 2k_3 + k_4) \tag{4.1}$$

with

$$k_1 = f(x_i, y_i) \tag{4.2}$$

$$k_2 = f(x_i + \frac{h}{2}, y_i + \frac{h}{2}k_1) \tag{4.3}$$

$$k_3 = f(x_i + \frac{h}{2}, y_i + \frac{h}{2}k_2) \tag{4.4}$$

$$k_4 = f(x_i + h, y_i + hk_3) \tag{4.5}$$

MatLab offers a standard library of ordinary differential equation solvers (ODE-Solver). The ode45-solver uses a refined version of the described Runge-Kutta method and was used for simulations in this thesis.

In MatLab, the function *pathway.m* was created. It contains the model-defining rate-law equations and calculates a numerical solution for a set time period. The resulting concentration changes can be plotted and the return value of the function is the final state of the system. The time period was chosen sufficiently large to ensure that the final state is a steady state.

The function *pathwayDR.m* calls the function *pathway.m* multiple times and varies the input parameters of the model (initial concentrations) to create Dose-Response-Curves.

4.2 Immunofluorescence imaging

Part of the thesis work involved realizing an experimental protocol to repeat the results of Miguez ([32], manuscript in preparation) and verify the model created and described here.

In [32], Míguez et al studied the AKT-pathway in a human renal cancer cell line (so called 786-O cells). The cells were engineered to stably express EGFP-FoxO1a, a fluorescent fusion protein that translocates from the cytoplasm to the nucleus in response to pathway deactivation. Due to the absence of PTEN in 786-O cells, the AKT pathway is constitutively active, which means that the EGFP-FoxO1a is constitutively localized in the cytoplasm. After pathway inhibition, EGFP-FoxO1a translocates the to the nucleus. Since it is possible that the fusion protein EGFP-FoxO1a behaves differently than unmodified FoxO1a, we tested an immunofluorescence approach for this thesis instead.

The cells used for the new experiments were again 786-O human renal cancer cells. The cells were cultured on standard p100 plates in DMEM F12 medium with Penicillin, Streptomycin and 7.5% FBS. DMEM and Trypsin/EDTA were supplied by the company VWR. Penicillin and Streptomycin were supplied by Sigma-Aldrich.

The culturing protocol can be found in full detail in section 8.1. To perform the immunofluorescence experiments, cells were fixed with Paraformaldehyde according to the protocol 8.2. Immunofluorescence staining was performed as described in 8.3.

Fluorescence microscopy was either performed in-house at Universidad Autonoma de Madrid (UAM) or at the "Centro de Biologia Molecular Severo Ochoa" (CBM).

At the CBM, a coupled microscope system was used, consisting of a inverted Zeiss Axiovert200M and a confocal Zeiss LSM510 using Argon and Helium lasers.

At UAM, the fluorescence microscope was a Leica DMI LED microscope. The objective was the Leica HI Plan I 20x/0.30 PH1. Imaging was done with the Leica DFC 3000 G camera on a ring c-mount 0.55x.

Chapter 5

Results

5.1 Modeling the PI3K/AKT/mTOR pathway

To investigate the role of the different members of the AKT-pathway, a mathematical model was simulated in MatLab. The model was designed to be as simple as possible while still showing the desired characteristics. On the other hand it was designed to be complicated enough to satisfy a sense of biological realism. This means the model does not contain arbitrary production and destruction of components, but activation and inactivation of a fixed amount of substances. Furthermore, reactions follow the laws of mass action and enzyme kinetics. These biochemical requirements strongly increase the number of variables (though they are connected by some conservation laws) even in a simple system.

As described in chapter 2, the AKT-PI3K-pathway can be sketched like this:

IRS1 (which has autocatalytic properties) activates PI3K, PI3K activates AKT, AKT activates mTOR, mTOR inhibits IRS1.

This could be further abstracted to the circuit shown in figure 5.2. This highly abstracted, reduced approach will be discussed later (chapter 6). To make the model biologically plausible, it has to account for:

1. Limited amounts of all the substances
2. Amounts cannot become negative
3. Interactions happen by forming complexes

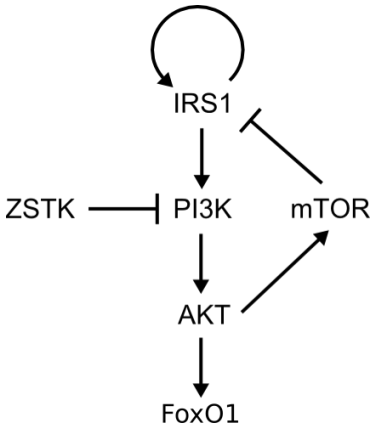

Figure 5.1: The AKT-pathway as described before.

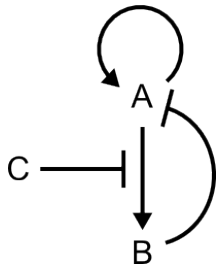

Figure 5.2: A very basic circuit that is structurally equivalent to the AKT-pathway.

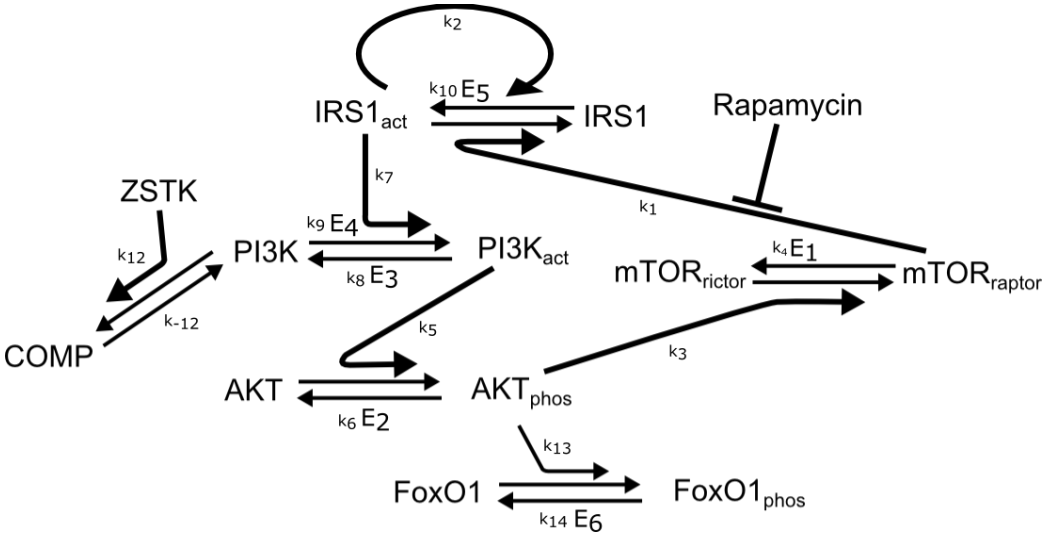

Figure 5.3: Graphical representation of the full pathway model

To incorporate the limited amounts, we make the assumption of a fixed amount of IRS1, PI3K, AKT, mTOR and FoxO, respectively. Instead of being produced and destroyed, the substances are modeled as changing from an "inactive" to an "active" state and vice versa.

To model the enzymatic activity, a Michaelis-Menten approach was used (see chapter 3.2). For all constituents of the pathway, we assume that the equilibrium between active and inactive state is the result of an activating and a deactivating enzyme. All enzyme interactions are modeled as proposed by Michaelis-Menten. Enzymes that were not part of the studied pathway (in the sense that they were not part of the network structure) were considered to stay at constant concentrations and labeled E_1 to E_6. The ZSTK-mediated inhibition of PI3K was modeled as PI3K and ZSTK forming a complex COMP that is passive in the pathway. The reaction was modeled following the law of mass action.

Figure 5.3 shows the graphic representation of the pathway as it was modeled. The rate-law equations are given as:

$$\frac{d[IRS1]}{dt} = k_1 \frac{[mTOR][IRS1_{act}]}{K_{m1} + [IRS1_{act}]} - k_2 \frac{[IRS1_{act}][IRS1]}{K_{m2} + [IRS1]} - k_{10} \frac{E_5[IRS1]}{K_{m10} + [IRS1]} \tag{5.1}$$

$$\frac{d[mTOR]}{dt} = k_3 * \frac{[AKT_{phos}] * [mTOR_{rictor}]}{(K_{m3} + [mTOR_{rictor}]} - k_4 * \frac{E_1 * [mTOR]}{(K_{m4} + [mTOR]} \tag{5.2}$$

$$\frac{d[AKT_{phos}]}{dt} = k_5 * \frac{[PI3K_{act}] * [AKT]}{K_{m5} + [AKT]} - k_6 * \frac{E_2 * [AKT_{phos}]}{(K_{m6} + [AKT_{phos}])} \tag{5.3}$$

$$\frac{d[PI3K]}{dt} = -k_7 * \frac{[IRS1_{act}]) * ([PI3K])}{K_{m7} + [PI3K]} + k_8 * \frac{E_3 * [PI3K_{act}]}{K_{m8} + [PI3K_{act}]} \\ -k_9 * \frac{E_4 * [PI3K]}{K_{m9} + [PI3K]} - k_{12} * [PI3K] * [ZSTK] + k_{-12} * [Comp] \tag{5.4}$$

$$\frac{d[Comp]}{dt} = k_{12} * [PI3K] * [ZSTK] - k_{-12} * [Comp] \tag{5.5}$$

$$\frac{d[FoxO_{phos}]}{dt} = k_{13} * \frac{[AKT_{phos}] * [FoxO]}{K_{m13} + [FoxO]} - k_{14} * \frac{E_6 * [FoxO_{phos}]}{K_{m14} + [FoxO_{phos}]} \tag{5.6}$$

To account for the influence of rapamycin, the factor $(1 - 0.5 * [Rapa])$ was multiplied with the first term of 5.1. For $[Rapa] = 0$, the factor is equal to 1 and has no influence. For $[Rapa] = 1$, the factor becomes $\frac{1}{2}$, so it weakens the negative feedback exerted by mTOR on IRS1.

For the actual computations, the number of variables was reduced by taking into account that the overall amount of each substance must be conserved (except rapamycin). So, $[IRS1_{act}]$ was replaced by $[IRS1_{tot}] - [IRS1]$, with $[IRS1_{tot}] = const.$ etc.

The full MatLab-Code can be found in 7.

Simulating this set of ODEs for several different initial conditions yields plots as in figure 5.4. In the first case (no ZSTK, figure 5.4a), the pathway is active, so after a little time, the system reaches a steady state in which $PI3K_{act}$, mTOR and FoxO are stably expressed. In the ZSTK-treated case (figure 5.4b), the concentrations of $PI3K_{act}$, mTOR and phosphorylated FoxO are greatly decreased, indicating successful pathway inhibition. Another very pronounced effect is the increase in IRS_{act} due to the absence of mTOR. Note that both simulations reach a steady state.

In the performed experiments, the drug ZSTK is the component that can directly be varied by the experimenter. FoxO is accessible to observation and the amount of nucleic FoxO (which is not phosphorylated) will therefore be regarded as the "response" of the system.

In figure 5.5, dose-response-curves are plotted. In figure 5.5a, the initial conditions where the individual components' concentrations when the system was allowed to reach a steady state with no ZSTK present (the final steady state of the simulation in figure 5.4a). In figure 5.5a, the steady state after treatment with ZSTK (figure 5.4b) was chosen as the initial steady state. For every single point of the curves in figure 5.5, new simulations were run with the initial conditions chosen as explained, and the ZSTK concentrations as noted on the x-axes.

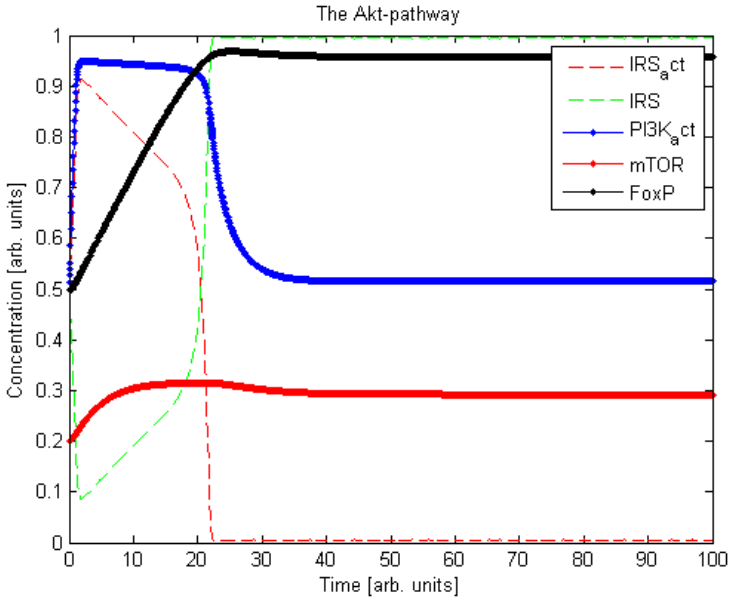

(a) No ZSTK present

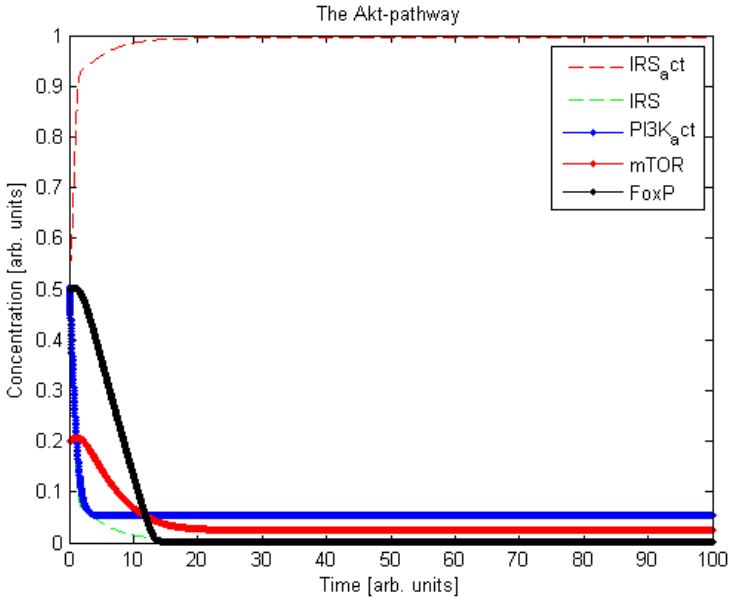

(b) ZSTK treatment

Figure 5.4: Simulation results of the AKT-pathway. Initial conditions were the same for both simulations, ecxept for the amount of ZSTK.

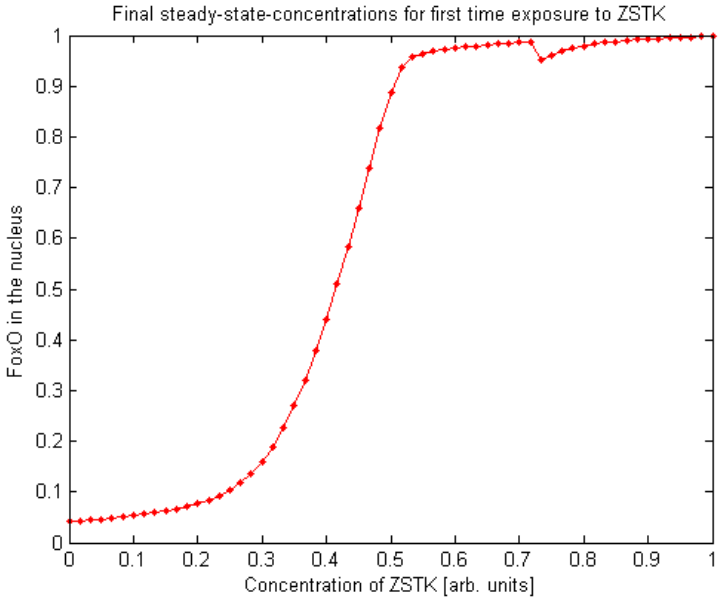

(a) Initially low ZSTK-steady-state

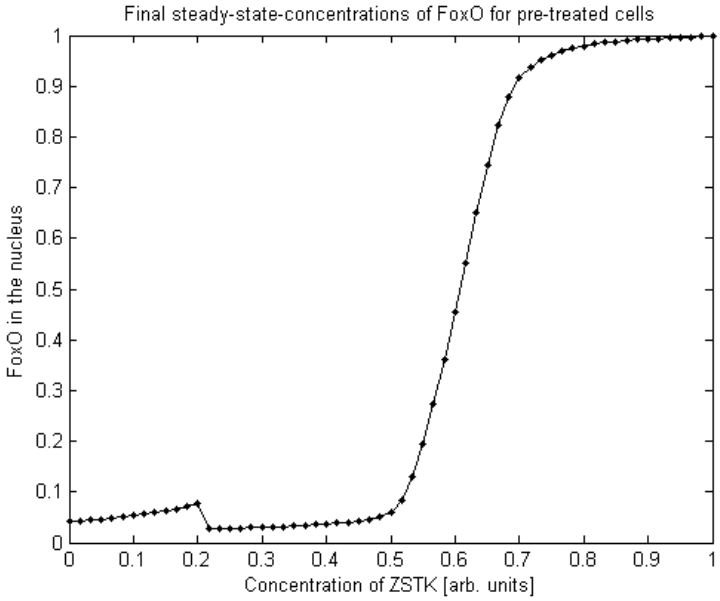

(b) Initially high ZSTK-steady-state

Figure 5.5: Simulated steady-state-concentrations of FoxO-phos in the AKT-pathway for different ZSTK concentrations

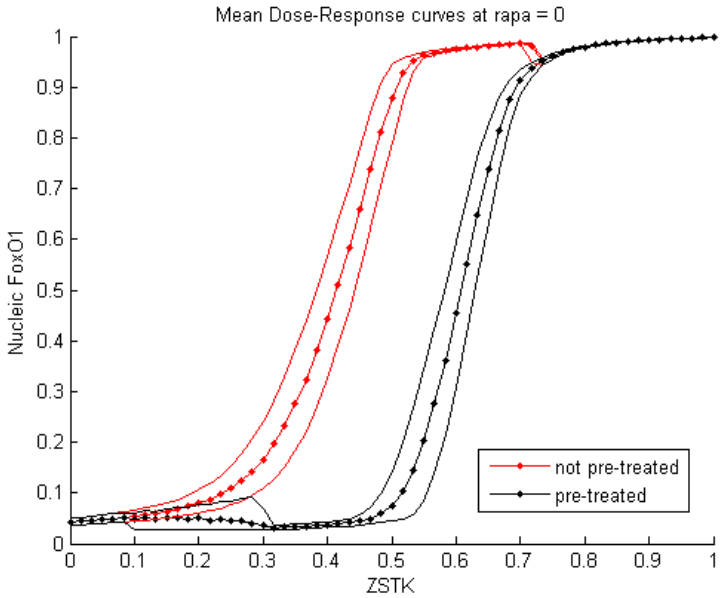

Figure 5.6: The average (mean) Dose-Response Curve for different expression levels of AKT (±5%). The light lines display the minimum/maximum responses.

In the actual experiments, a multitude of cells has to be observed. Naturally, these cells vary in size, health and expression levels of proteins, including AKT. To account for this natural variation of cell phenotypes, the simulations were run for different values of overall AKT. Figure 5.6 shows the averaged Dose-Response-Curve which is closer to what can be expected to be observed in the experiment than figure **??**.

Figure 5.7 shows the effect of rapamycin on the system. Note that the curves are not only shifted towards higher concentrations of ZSTK, but also the change from proteretic to hysteretic behavior.

5.2 The immunofluorescence images

A number of immunofluorescence staining protocols was tested (see sections 8). Unfortunately, no quantifiable results were achieved.

Figures 5.8 and 5.9 exemplarily show the results for incubation with no ZSTK and with a high amount (5 µM) of ZSTK, respectively.

Addition of ZSTK is expected to inhibit PI3K (see section 2.2), thereby decreasing the activity of the AKT-pathway. This in turn leads to reduced

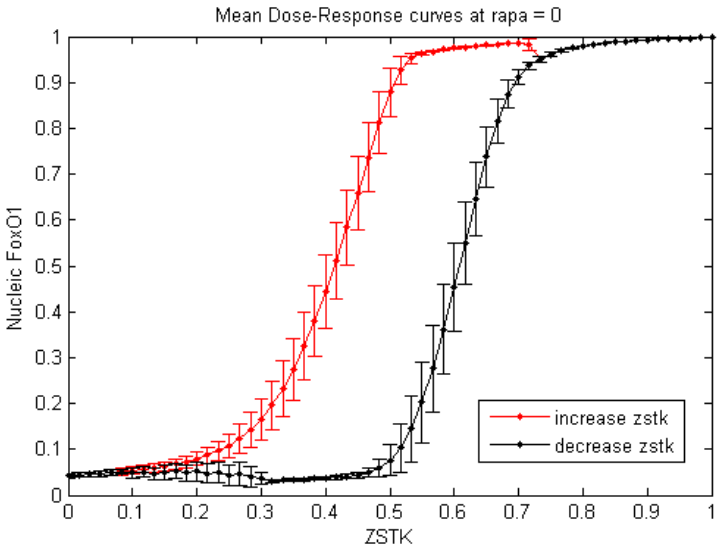

(a) Rapamycin = 0

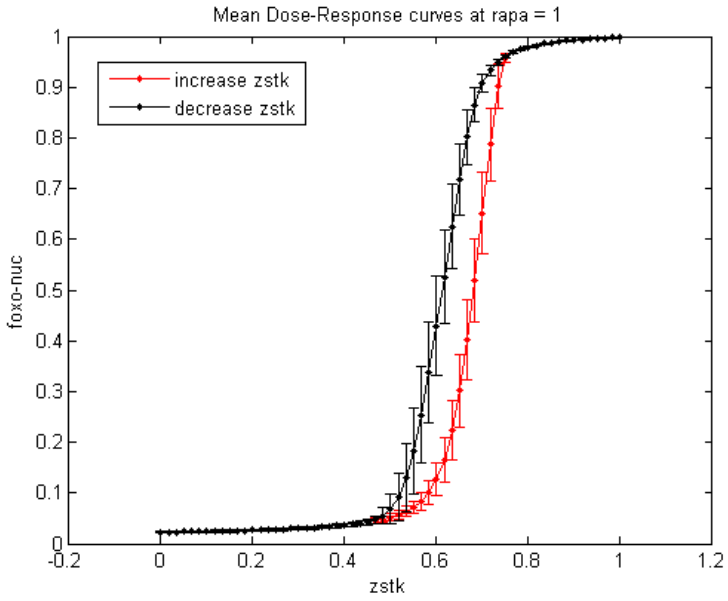

(b) Rapamycin = 1

Figure 5.7: Dose-Response Curves for two levels of rapamycin. The error-bars show standard deviations resulting from variation of overall AKT-expression. The left figure results from the same simulation as fig. 5.6. For the right figure (5.7b), the negative feedback via mTOR is reduced to half its strength by setting the rapamycin-variable to 1 (arb. unit).

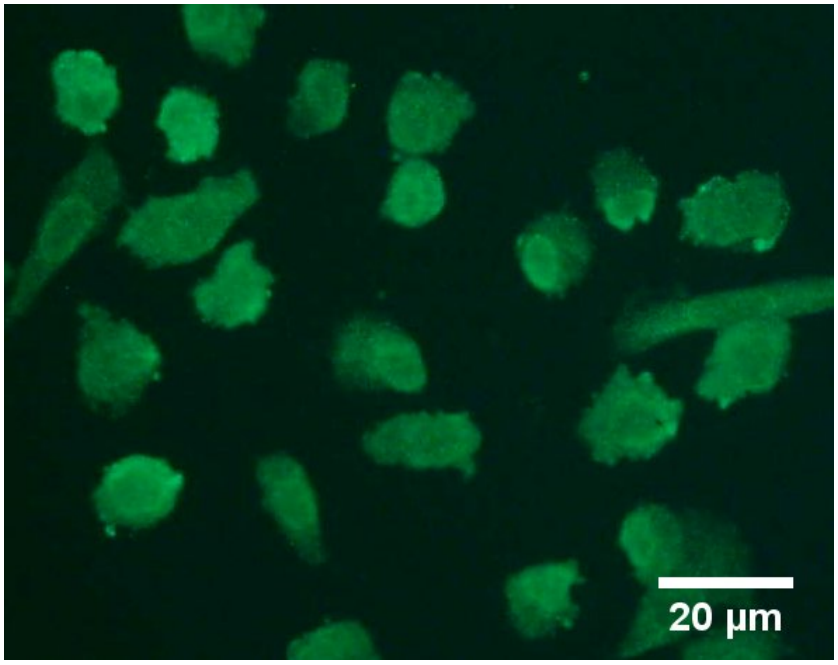

Figure 5.8: Immunofluorescence image of 786-O cells. FoxO1 is shown in green and is evenly distributed in the cell.

phosphorylation of FoxO1. This leads to increased migration of FoxO1 to the nucleus. Qualitatively, this can be observed in the two images (fig. 5.8 and 5.9).

The effect was not sufficiently pronounced to allow for quantification.

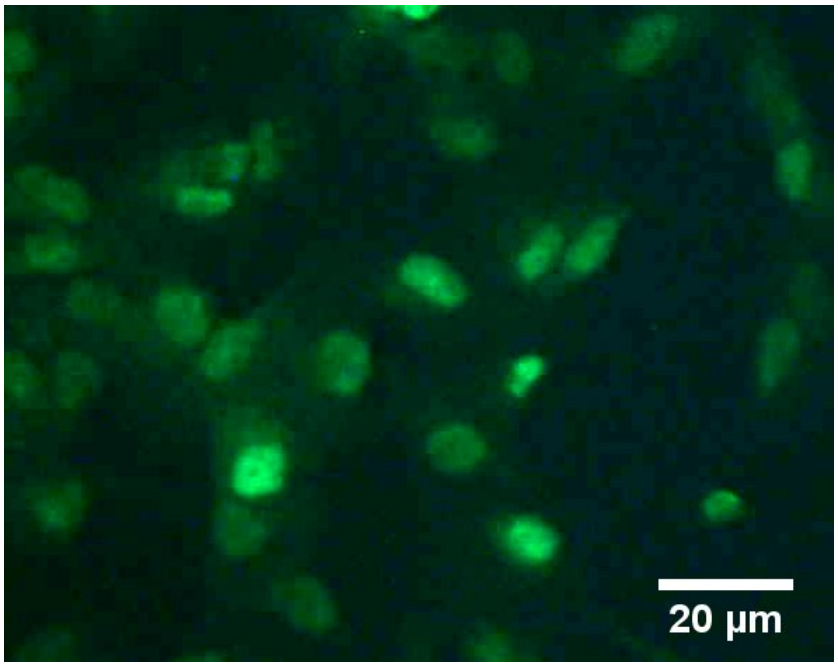

Figure 5.9: Immunofluorescence image of 786-O cells treated with ZSTK. FoxO1 is shown in green and is concentrated in the nucleus.

Chapter 6

Discussion and Outlook

6.1 The AKT-pathway

As shown in the results, proteretic behavior can occur in cellular signaling pathways. This has consequences for drug scheduling in cancer therapy. The proteretic behavior is equivalent to a de-sensitization of the system: The same dose will create less response when applied shortly after the former dose.

The architecture found in the modeled AKT-pathway can be thought of consisting only of:

1. A negative feedback-loop
2. A positive auto-catalytic loop
3. Non-linearities

These ingredients are sufficient to create proteretic behavior in a certain parameter range. In contrast, hysteretic behavior only needs non-linearities and negative feedback.

The simulations indicate that Rapamycin removes the proteretic behavior from the pathway. Further, it decreases the sensitivity of the system to treatment with ZSTK. Both observations are in accordance with the unpublished results from D.G. Míguez ([32], figure 6.1). This suggests that combined treatment with both drugs might be more reliable and less schedule-dependent, but require higher doses.

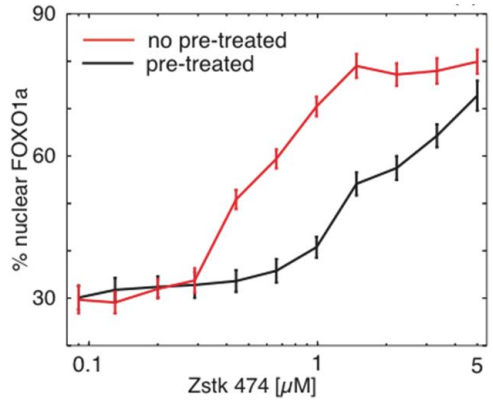

Figure 6.1: Experimental dose-response curves, showing that pretreated cells become desensitized for a wide range on ZSTK474 concentration

6.2 Experimental Procedure

As shown in the experimental results, the addition of ZSTK inhibits the AKT pathway and the strength of the inhibition can in principle be monitored by monitoring the migration of FoxO1 to the cell nucleus. However, our approaches to image FoxO1 by immunofluorescence did not yield quantifiable results.

However, quantifiable results are essential to test the predictions of the presented model (5.1). Especially the supposed occurrence of inverted hysteresis calls for very precise and robust quantification to rule out random errors as the reason for differences between the untreated and pre-treated dose-response-curves.

Engineering GFP (green fluorescent protein) to FoxO1 might be a reasonable experiment, as this produced the results that motivated this thesis. Repeating those experiments with higher precision and in a new setup should provide new insights.

The drawback of the GFP-approach lies in the alteration of the target molecule. It is difficult to decide whether an effect would also occur with the unmodified molecule.

Once the results can be reproduced with 786-O cells, it will be interesting to test the same pathway in other cell lines.

6.3 Inverted Hysteresis in general

The question remains whether simpler systems can exhibit proteretic behavior. Identifying more proteretic systems might aid in defining *necessary* ingredients for proteretic behavior.

A more profound understanding of this exotic behavior would also allow to make definite statements about a pathway's architecture. If a pathway displays proteretic behavior in a dose-response experiment, it might be safe to say, for instance, that there must be some kind of negative feedback loop in the pathway. Identifying such a negative feedback could then open up new methods to alter the pathway's activity.

Chapter 7

MatLab-Code

7.1 The model

```
function [ y_fin ] = akt_model(akt_tot,all_init,zstk,rapa)
% akt_model.m
% This function runs the actual simulation the Akt-pathway.
% The pathway is modeled as a set of differential equations that are
% numerically solved using the modified Runge-Kutta-algorithm supplied
% by MatLab under the name "ode45".

% The return value "y_fin" is a vector containing the final state of the
% system.



%% Plotting on/off
plot_on = 0;

%% Parameters
k1 = 4;   % reaction irs act --> irs, enzyme mTOR
km1 = 0.11;

k2 = 2;   % reaction irs --> irs-act, enzyme irs-act (autocatalysis)
km2 = 0.11;

k10 = 1;  % small "native" irs-act-production, so steady-state not zero
km10 = 0.11;
E5 = 0.05;

k3 = 1;   % rictor --> mTOR, enzyme AKTP
km3 = 0.11;
```

```
k4 = 1;   % mTOR --> rictor, mediated by constant enzyme E1
km4 = 0.11;
E1 = 0.05;

k5 = 1;   % akt -> akt-p reaction, enzyme PI3K_act
km5 = 0.11;

k6 = 1;   % akt-p --> akt, enzyme E2 (constant)
km6 = 0.11;
E2 = 0.25;

k7 = 1;   % PI3K --> PI3K_act, enzyme IRS_act
km7 = 0.11;

k8 = 1;   % PI3K_act --> PI3K, constant enzyme E3
km8 = 0.11;
E3 = 0.5;

k9 = 1;   % equilibrate PI3K<->PI3K act, enz. E4
km9 = 0.11;
E4 = 0.5;

k12 = 100; % PI3K + ZSTK -> COMP (inhibition of PI3K by ZSTK)
k_12 = 0.1;

k13 = 1;   % Fox -> FoxP by AKTP
km13 = 0.01;

k14 = 1;   % FoxP -> Fox by E6
km14 = 0.01;
E6 = 0.06;

constants=[k1,km1,k2,km2,k3,km3,k4,km4,k5,km5,k6,km6,k7,km7,k8,km8,...
k12,k_12,k13,km13,k14,km14,E1,E2,E3,E4,E5,E6];

%% initial conditions:

man_init = 1;

if man_init == 1

IRS_tot = 1;
IRS_0 = 0.5;

mTOR_tot = 0.4;
mTOR_0 = 0.2;
%rictor_0 = mTOR_tot - mTOR_0;

AKT_tot = akt_tot;
```

```
AKTP_0 = 0.05;
AKT_0 = AKT_tot - AKTP_0;

PI3K_tot = 1;
PI3K_act_0 = 0.5;
PI3K_0 = PI3K_tot - PI3K_act_0;

ZSTK_0 = zstk;

COMP_0 = 0;

Fox_tot = 1;
FoxP_0 = 0.5;

end

%% Solve ODEs to get initial state

tspan = [0,100];

init = all_init;
%init = [IRS 0 mTOR 0 AKTP 0 PI3K 0 COMP 0 FoxP 0];
%init = [IRS 0 mTOR 0 AKTP 0 PI3K 0 COMP 0 FoxP 0];
options = [];

[t,y] = ode45(@irs_fun,tspan,init,options,constants,rapa);

%% Define the function


    function dydt = irs fun(t,y,constants,rapa)
        IRS = y(1);
        mTOR = y(2);
        AKTP = y(3);
        PI3K = y(4);
        COMP = y(5);
        FoxP = y(6);


dydt = [
    k1*(1-0.5*rapa)*mTOR*(IRS_tot-IRS)/(km1+IRS_tot-IRS)-...
         k2*(IRS_tot-IRS)*IRS/(km2+IRS) - k10*E5*IRS/(km10+IRS); %IRS
    k3*AKTP*(mTOR_tot-mTOR)/(km3+mTOR_tot-mTOR) -...
         k4*E1*mTOR/(km4+mTOR); %mTOR
    k5*(PI3K_tot-COMP-PI3K)*(AKT_tot-AKTP)/(km5+AKT_tot-AKTP)-...
         k6*E2*AKTP/(km6+AKTP); %AKTP
    -k7*(IRS_tot-IRS)*(PI3K)/(km7+PI3K) +...
         k8*E3*(PI3K_tot-PI3K-COMP)/(km8+PI3K_tot-PI3K-COMP) -...
         k9*E4*PI3K/(km9+PI3K) - k12*PI3K*(ZSTK_0-COMP) + k_12*COMP; %PI3K
```

```
    k12*PI3K*(ZSTK_0-COMP) - k_12*COMP; %COMP
    k13*AKTP*(Fox_tot-FoxP)/(km13+Fox_tot-FoxP) -...
         k14*E6*FoxP/(km14+FoxP)]; %FoxP


    end

%% Preparing the results

       IRS = y(:,1);
       IRS_act = IRS_tot - IRS;
       mTOR = y(:,2);
       rictor = mTOR tot - mTOR;
       AKTP = y(:,3);
       AKT = AKT_tot - AKTP;
       PI3K = y(:,4);
       COMP = y(:,5);
       PI3K_act = PI3K_tot - PI3K - COMP;
       ZSTK = ZSTK_0 - COMP;
       FoxP = y(:,6);


       y_fin = y(end,:); % The return values, for akt model DR.m

%% Plotting
if plot_on == 1

figure()

plot(t,IRS act,'--r',t,IRS,'--g',t,PI3K act,'.-b',t,mTOR,'.-r',...
    t,FoxP,'.-k');
legend('IRS_act','IRS','PI3K_act','mTOR','FoxP');
xlabel('Time [arb. units]');
ylabel('Concentration [arb. units]');
title('The Akt-pathway');

end

end
```

7.2 The Dose-Response-Curves

```
function [output] = akt_model_DR(AKT,rapa)
% akt_model_DR collects data twice:
% 1st run: starts in steady state (achieved after running one
% simulation), then increases ZSTK (starts a new simulation
% for each ZSTK concentration, each time starting from the
```

```
% initially achieved steady state)

% 2nd run: starts in a steady state achieved after "treatment"
% with ZSTK, then decreases ZSTK, everytime from the same
% initial steady state
%

%% Parameters
ZSTK_points = linspace(0,1,61); %evenly spaced ZSTK-concentrations
ZSTK_points_rev = fliplr(ZSTK_points);

akt_tot = AKT;

%% Evaluate the ODEs

% 1st run
% "high_init" refers to high expression of akt-p -> zstk is low
high_init = akt_model(akt_tot,[0.5 0.2 0.05 0.5 0 0.5],0,rapa);

val_inc = zeros(size(ZSTK_points,2),size(high_init,2));
val_dec = zeros(size(ZSTK_points,2),size(high_init,2));

for i=1:size(ZSTK_points,2)

    init = high_init;
    zstk = ZSTK_points(i); %set zstk to next point
    init(4) = init(4) + init(5); %add COMP to PI3K
    init(5) = 0; %clear COMP

    val_inc(i,:)=akt_model(akt_tot,init,zstk,rapa);
end

% 2nd run
% "low_init" refers to low expression of akt-p -> zstk is high
low_init = akt_model(akt tot,[0.5 0.2 0.05 0.5 0 0.5],1,rapa);

for i=1:size(ZSTK points,2)

    init = low_init;
    zstk = ZSTK_points_rev(i); %set zstk to next point
    init(4) = init(4) + init(5); %add COMP to PI3K
    init(5) = 0; %clear COMP

    val_dec(i,:)=akt_model(akt tot,init,zstk,rapa);
end


%% Plot the dose-response curves
```

```
irs1_act_inc_ZSTK = 1-val_inc(:,1);
irs1_act_dec_ZSTK = 1-val_dec(:,1);

mTOR_inc_ZSTK = val_inc(:,2);
mTOR_dec_ZSTK = val_dec(:,2);

aktp_inc_ZSTK = val_inc(:,3);
aktp_dec_ZSTK = val_dec(:,3);

pi3k_act_inc_ZSTK = 1-val_inc(:,4)-val_inc(:,5);
pi3k_act_dec_ZSTK = 1-val_dec(:,4)-val_dec(:,5);

nuc_fox_inc = 1 - val_inc(:,6);
nuc_fox_dec = 1 - val_dec(:,6);

output = [nuc_fox_inc,nuc_fox_dec];

plot_switch = 0; % to limit which plots are executed
if plot_switch == 1

figure()
plot(ZSTK_points,irs1_act_inc_ZSTK,'.-r',...
    ZSTK_points_rev,irs1_act_dec_ZSTK,'.-b')
legend('increase zstk','decrease zstk')
xlabel('zstk')
ylabel('irs1-act')
title(['Dose-Response curves at rapa = ',num2str(rapa)])

figure()
plot(ZSTK_points,mTOR_inc_ZSTK,'.-r',...
    ZSTK_points_rev,mTOR_dec_ZSTK,'.-b')
legend('increase zstk','decrease zstk')
xlabel('zstk')
ylabel('mTOR')
title(['Dose-Response curves at rapa = ',num2str(rapa)])

figure()
plot(ZSTK_points,aktp_inc_ZSTK,'.-g',...
    ZSTK_points_rev,aktp_dec_ZSTK,'.-r')
legend('increase zstk','decrease zstk')
xlabel('zstk')
ylabel('aktp')
title(['Dose-Response curves at rapa = ',num2str(rapa)])

figure()
plot(ZSTK_points,pi3k_act_inc_ZSTK,'.-b',...
    ZSTK_points_rev,pi3k_act_dec_ZSTK,'.-k')
legend('increase zstk','decrease zstk')
xlabel('zstk')
```

```
ylabel('pi3k-act')
title(['Dose-Response curves at rapa = ',num2str(rapa)])

figure()
plot(ZSTK_points,nuc_fox_inc,'.-r',...
    ZSTK_points_rev,nuc_fox_dec,'.-k')
legend('increase zstk','decrease zstk')
xlabel('zstk')
ylabel('foxo')
title(['Dose-Response curves at rapa = ',num2str(rapa)])

figure()
plot(ZSTK_points,nuc_fox_inc,'.-r')
xlabel('Concentration of ZSTK [arb. units]')
ylabel('FoxO in the nucleus')
title('Final steady-state-concentrations'...
    ' for first time exposure to ZSTK')

figure()
plot(ZSTK_points_rev,nuc_fox_dec,'.-k')
xlabel('Concentration of ZSTK [arb. units]')
ylabel('FoxO in the nucleus')
title('Final steady-state-concentrations'
    ' of FoxO for pre-treated cells')

figure()
plot(ZSTK_points,nuc_fox_inc,'.-r',...
    ZSTK_points_rev,nuc_fox_dec,'.-k')
legend('No pre-treatment','pre-treated cells')
xlabel('Concentration of ZSTK [arb. units]')
ylabel('FoxO')
title('The complete Dose-Response-Curve')

end % Move this "end" to decide what is plotted

end
```

7.3 The averaging over different total amounts of AKT

```
function [] = DR_avg()
% This program runs akt_model_DR a few times, varying akt_tot,
% thereby varying the resulting fox_o curves. (Varying akt_tot shall
% account for different cells, which may express different natural
% levels of AKT)
%
```

```
% Furthermore, the Rapamycin-Parameter can be chosen in this program
% and handed down to the model
%

%% Parameters

rapa = 0;

N_akt = 7; % Defines, how many akt-levels are to be simulated

AKT_vary = linspace(0.097,0.103,N_akt); % Evenly spaced akt-levels


%% Run the DR simulations

testo = akt_model_DR(0.1,rapa); % running one test-simulation

val_inc = zeros(size(testo,1),N akt); % assign a matrix of correct size
val_dec = zeros(size(testo,1),N akt);

for j=1:N_akt

    temp = akt_model_DR(AKT_vary(j),rapa);
    val_inc(:,j) = temp(:,1);
    val_dec(:,j) = temp(:,2);

end

zstk_guess = linspace(0,1,size(testo,1));


val_inc_med = median(val_inc,2);
val_inc_mean = mean(val_inc,2);
val_inc_dev = std(val_inc,1,2);
val_inc_min = min(val_inc,[],2);
val_inc_max = max(val_inc,[],2);

val_dec_med = median(val_dec,2);
val_dec_mean = mean(val_dec,2);
val_dec_dev = std(val_dec,1,2);
val_dec_min = min(val_dec,[],2);
val_dec_max = max(val_dec,[],2);


%% Plot the dose-response curves

% Figures with standard deviation

figure()
```

```
errorbar(zstk_guess,val_inc_med,val_inc_dev,'.-r')
hold on
errorbar(fliplr(zstk_guess),val_dec_med,val_dec_dev,'.-k')
legend('not pre-treated','pre-treated')
xlabel('ZSTK')
ylabel('Nucleic FoxO1')
title(['Median Dose-Response curves at rapa = ',num2str(rapa)])
hold off

figure()
errorbar(zstk_guess,val_inc_mean,val_inc_dev,'.-r')
hold on
errorbar(fliplr(zstk_guess),val_dec_mean,val_dec_dev,'.-k')
legend('not pre-treated','pre-treated')
xlabel('ZSTK')
ylabel('Nucleic FoxO1')
title(['Mean Dose-Response curves at rapa = ',num2str(rapa)])
hold off

% Figures mean/median ONLY
figure()
plot(zstk guess,val_inc_med,'.-r',fliplr(zstk_guess),val_dec_med,'.-k')
legend('not pre-treated','pre-treated')
xlabel('ZSTK')
ylabel('Nucleic FoxO1')
title(['Median Dose-Response curves at rapa = ',num2str(rapa)])

figure()
plot(zstk_guess,val_inc_mean,'.-r',fliplr(zstk_guess),val_dec_mean,'.-k')
legend('not pre-treated','pre-treated')
xlabel('ZSTK')
ylabel('Nucleic FoxO1')
title(['Mean Dose-Response curves at rapa = ',num2str(rapa)])

% Figures with min-max
figure()
hold on
plot(zstk_guess,val_inc_med,'.-r',fliplr(zstk_guess),val_dec_med,'.-k')
plot(zstk_guess,val_inc_min,'-r',fliplr(zstk_guess),val_dec_min,'-k')
plot(zstk_guess,val_inc_max,'-r',fliplr(zstk_guess),val_dec_max,'-k')
legend('not pre-treated','pre-treated')
xlabel('ZSTK')
ylabel('Nucleic FoxO1')
title(['Median Dose-Response curves at rapa = ',num2str(rapa)])
hold off

figure()
hold on
plot(zstk_guess,val_inc_mean,'.-r',fliplr(zstk_guess),val_dec_mean,'.-k')
```

```
plot(zstk_guess,val_inc_min,'-r',fliplr(zstk_guess),val_dec_min,'-k')
plot(zstk_guess,val_inc_max,'-r',fliplr(zstk_guess),val_dec_max,'-k')
legend('not pre-treated','pre-treated')
xlabel('ZSTK')
ylabel('Nucleic FoxO1')
title(['Mean Dose-Response curves at rapa = ',num2str(rapa)])
hold off

end
```

Chapter 8

Lab-Protocols

The cells used were 786-O cells and they were handled according to the following protocols:

8.1 Passing the cells

1. Discard old medium
2. Wash with PBS (37 °C)
3. Add 1.7 ml Trypsin+EDTA (37 °C)
4. Make sure all the cells detach from the plate
5. Deactivate Trypsin+EDTA by adding 2 ml complete DMEM + Pen/Strep + 7.5%FBS (37 °C)
6. Wash the plate with the DMEM and transfer the cells to a falcon tube.
7. Repeat step 6 with 2 ml of DMEM
8. Centrifuge for 5 minutes at 1500 rpm
9. Discard media with vacuum device
10. Resuspend the cells in complete DMEM
11. Seed to new plate

8.2 Fixing the cells for immunos

1. Grow cells on coverslips in 12-well plate (1/20 the area of a p100 plate), therefore dilution of 1:20 or 1:40 works well (1:20 gave quite a high density)
2. Wait over night, so the cells adhere to the coverslip
3. Actual fixing:
4. Discard medium with vacuum device
5. OPTIONAL: Wash with PBS 1x
6. Fix with 1 ml of 4% Paraformaldehyde in PBS
7. Wait for 15 minutes at room temperature
8. Discard PBS-PFA with vacuum device
9. NOT OPTIONAL: Wash a few times with PBS
10. Keep in PBS 1x at 4 °C in the fridge

8.3 Immuno first try at CBM 23. + 24.10.2014

1. Prepare PBS with 3% BSA, prepare methanol/triton
2. Prepare cells as described in 8.2
3. Remove PBS using a vacuum device, placing the tip in the edge of the well
4. Permeabilization:
   - Option a: done for two samples: Methanol permeabilization: 700 µl of −20 °C methanol for 5 minutes.
   - Option b: done for two samples, according to Jaime probably the better option: 700 µl of triton 4 °C for 5 minutes at 4 °C
5. Wash with PBS after permeabilization!!
6. Blocking: Remove the PBS, add PBS with 3% BSA and wait for minimum 10 minutes at room temperature (note: longer does not matter, prepare BSA early, because the homogeneous distribution takes a long time)

7. While blocking, prepare humidity chamber: e.g. p100 plate with filter paper + parafilm
8. Prepare primary antibody(ies): Dilute AB in PBS+BSA!! Optional: Also add Topro or Phalloidin (only compatible with triton permeabilization) Prepare 30 µl per coverslip
9. Place one 25 µl droplet per coverslip on the parafilm in the humidity chamber
10. Take coverslip from the 12-well plate (tweezers) and wash 30 times in bowl of PBS
11. Place coverslip on drop of primary antibody.
12. Leave overnight at room temperature (? or was it the fridge?) (probably also possible: waiting 1 hour at 37 °C)
13. Prepare secondary antibodies in PBS+BSA and put drops on second humidity chamber (just as with the primary AB)
14. Wash coverslips 30 times in PBS, place on secondary-AB drops
15. Wait 30 minutes at 37 °C
16. Wash again and put on 9 µl fluoromont/mowiol drops
17. Remove unnecessary fluoromont/mowiol with paper
18. Wait over night at room temperature

8.4 Immuno second try at CBM 12. + 13.11.2014

1. Prepare PBS with 3% BSA, prepare Triton 0.2%
2. Prepare cells as described in 8.2
3. Remove PBS using a vacuum device, placing the tip in the edge of the well
4. Permeabilization: 1 ml of triton at 4 degrees for 5 minutes at 4 degree
5. Wash with PBS after permeabilization!!

6. Blocking: Remove the PBS, add PBS with 3% BSA and wait for minimum 10 minutes at room temperature (note: longer does not matter, prepare BSA early, because the homogeneous distribution takes a long time)

7. While blocking, prepare humidity chamber: e.g. p100 plate with filter paper + parafilm, use distilled water!

8. Prepare primary antibody(ies): Dilute AB in PBS+BSA!! anti foxo1 1:50 (3 samples), 1:25 (1 sample): diluted 2.4/1.6 microlitres in 120/40 microlitres, respectively. also anti-tubulin-ab from CBM.

9. Place one 30 µl droplet per coverslip on the parafilm in the humidity chamber

10. Take coverslip from the 12-well plate (tweezers)

11. Place coverslip on drop of primary antibody.

12. Leave overnight in the fridge at 4 °C (probably also possible: waiting 1 hour at 37 degrees)

13. Prepare secondary antibody(ies) in PBS+BSA and put 30 µl drops on humidity chamber (just as with the primary AB)(prepare 40 µl per sample). we used FITC anti-rabbit secondary AB for FoxO1-staining at 1:25 dilution and anti-mouse 555 nm for tubulin-staining.

14. Wash coverslips 30 times in PBS, place on 2nd AB drops

15. Wait 30 minutes at 37 °C

16. Prepare DAPI 1:1000, 30 ul drops again

17. Incubate for 15 minutes at 37 °C.

18. Wash again and put on 9 µl moviol drops

19. Remove unnecessary fluoromont/moviol with paper

20. Wait 1-2 h at 37 °C

21. Store at 4 °C

8.5 Immuno third try at UAM 20.-25.11.2014

1. At least one day before! Prepare PBS with 3% BSA:
   - BSA is a powder that is stored in the fridge
   - To prepare 3% PBS-BSA solution dissolve 3g BSA in 100 ml PBS
   - Weigh the proper amount using the fine scale
   - Pour in small amount of PBS, then add the rest of PBS
   - Agitate using the agitator
   - Leave in fridge for some hours for the BSA to dissolve completely and diffuse homogeneously.
2. Prepare Triton 0.2%
   - Triton is a very viscous liquid that is stored in the chemicals wardrobe
   - Prepare a stock aliquote
   - To prepare the 0.2% solution, use Triton from the stock aliquote
   - Dissolve in PBS: Works better when PBS is warm, start inverting the tube as soon as possible
3. Prepare cells as described in 8.2 - also a day before.
4. Remove PBS using a vacuum device, placing the tip in the edge of the well
5. Permeabilization: 1 ml of triton at 4 °C for 5 minutes at 4 °C
6. Wash with PBS after permeabilization!
7. Blocking: Remove the PBS, add PBS with 3% BSA and wait for minimum 10 minutes at room temperature (note: longer does not matter)
8. While blocking, prepare humidity chamber: p100 plate with filter paper + parafilm (sticky side up), use distilled water!
9. Prepare primary antibody(ies): Dilute AB in PBS+BSA!! New anti-FoxO1 (Cell Signaling Technologies FoxO1 (C29H4) Rabbit mAB) 1:100 (all samples), mouse serum 1:50 (4 samples): Prepare 4 drops with FoxO1 and mouse serum and 2 drops with only FoxO, calculated 25 µl per drop plus 10 µl for pipetting errors.

10. Place one 25 µl droplet per coverslip on the parafilm in the humidity chamber
11. Take coverslip from the 12-well plate (tweezers)
12. Place coverslip on drop of primary antibody (cells facing the antibody).
13. Leave overnight in the fridge at 4 °C (probably also possible: waiting 1 hour at 37 degrees)
14. Prepare secondary antibody(ies) in PBS+BSA and put 25 µl drops on humidity chamber (just as with the primary AB). All samples used anti-mouse-555 1:500 (from the other lab), half the samples anti-rabbit(FoxO1)-488 1:25 from our lab, half the samples anti-rabbit(FoxO1)-488 1:500 from the other lab.
15. Wash coverslips 30 times in PBS, place on secondary AB drops
16. Incubate 30 minutes at 37 °C
17. Prepare DAPI 1:1000, 25 µl drops again
18. Incubate for 15 minutes at 37 °C.
19. Wash again and put on 9 µl mowiol drops
20. Remove unnecessary fluoromont/mowiol with paper
21. Wait overnight at room temperature.
22. Store at 4 °C

8.6 Immuno fourth try at CBM around 3.-5.12.2014

1. At least one day before! Prepare PBS with 3% BSA:
    - BSA is a powder that is stored in the fridge
    - To prepare 3% PBS-BSA solution dissolve 3g BSA in 100 ml PBS
    - Weigh the proper amount using the fine scale
    - Pour in small amount of PBS, then add the rest of PBS
    - Agitate using the agitator

- Leave in fridge for some hours for the BSA to dissolve completely and diffuse homogeneously.

2. Prepare Triton 0.2%
   - Triton is a very viscous liquid that is stored in the chemicals wardrobe
   - Prepare a stock aliquote
   - To prepare the 0.2% solution, use Triton from the stock aliquote
   - Dissolve in PBS: Works better when PBS is warm, start inverting the tube as soon as possible
3. Prepare cells as described in 8.2 - also a day before.
4. Remove PBS using a vacuum device, placing the tip in the edge of the well
5. Permeabilization: 1 ml of triton at 4 °C for 5 minutes at 4 °C
6. Wash with PBS after permeabilization!!
7. Blocking: Remove the PBS, add PBS with 3% BSA and wait for minimum 10 minutes at room temperature (note: longer does not matter)
8. While blocking, prepare humidity chamber: p100 plate with filter paper + parafilm (sticky side up), use distilled water!
9. Prepare primary antibody(ies)(see spreadsheet).
10. Place one 25 µl droplet per coverslip on the parafilm in the humidity chamber
11. Take coverslip from the 12-well plate (tweezers)
12. Place coverslip on drop of primary antibody (cells facing the antibody).
13. Leave overnight in the fridge at 4 °C (probably also possible: waiting 1 hour at 37 degrees)
14. Prepare secondary antibody(ies) in PBS+BSA and put 25 µl drops on humidity chamber (just as with the primary AB). All samples used anti-mouse-555 1:500 (from the other lab), half the samples anti-rabbit(FoxO1)-488 1:25 from our lab, half the samples anti-rabbit(FoxO1)-488 1:500 from the other lab.

15. Wash coverslips 30 times in PBS, place on secondary AB drops
16. Incubate 30 minutes at 37 °C
17. Wash 30 times in PBS
18. Prepare DAPI 1:1000, 25 µl drops again
19. Incubate for 15 minutes at 37 °C.
20. Wash again and put on 9 µl mowiol drops
21. Push coverslip lightly into the mowiol with the tweezers
22. Remove unnecessary fluoromont/mowiol with paper
23. Wait overnight at 4 °C
24. Store at 4 °C

8.7 Immuno fifth try at UAM around 14.-16.12.2014 and sixth try 21.-23.1.2015 and also seventh 27.-29.1.2015

1. At least one day before! Prepare PBS with 3% BSA:
   - BSA is a powder that is stored in the fridge
   - To prepare 3% PBS-BSA solution dissolve 3g BSA in 100 ml PBS
   - Weigh the proper amount using the fine scale
   - Pour in small amount of PBS, then add the rest of PBS
   - Agitate using the agitator
   - Leave in fridge for some hours for the BSA to dissolve completely and diffuse homogeneously.
2. Prepare Triton 0.2%
   - Triton is a very viscous liquid that is stored in the chemicals wardrobe
   - Prepare a stock aliquote
   - To prepare the 0.2% solution, use Triton from the stock aliquote

- Dissolve in PBS: Works better when PBS is warm, start inverting the tube as soon as possible

3. Prepare cells as described in 8.2 - also a day before.
4. Remove PBS using a vacuum device, placing the tip in the edge of the well
5. Permeabilization: 1 ml of triton at 4 °C for 5 minutes at 4 °C
6. Wash with PBS after permeabilization!!
7. Blocking: Remove the PBS, add PBS with 3% BSA and wait for minimum 10 minutes at room temperature (note: longer does not matter)
8. While blocking, prepare humidity chamber: p100 plate with filter paper + parafilm (sticky side up), use distilled water!
9. Prepare primary antibody(ies): Dilute AB in PBS+BSA!! calculate e.g. 25 µl per drop plus 10 µl for pipetting errors.
10. Place one 25 µl droplet per coverslip on the parafilm in the humidity chamber
11. Take coverslip from the 12-well/24-well(immuno6) plate (tweezers)
12. Place coverslip on drop of primary antibody (cells facing the antibody).
13. Leave overnight in the fridge at 4 °C (probably also possible: waiting 1 hour at 37 degrees)
14. Prepare secondary antibody(ies) in PBS+BSA and put 25 µl drops on humidity chamber (just as with the primary AB). All samples used anti-mouse-555 1:500 (from the other lab), half the samples anti-rabbit(FoxO1)-488 1:25 from our lab, half the samples anti-rabbit(FoxO1)-488 1:500 from the other lab.
15. Wash coverslips 30 times in PBS, place on secondary AB drops
16. Incubate 30 minutes at 37 °C
17. Wash 30 times in PBS
18. Prepare DAPI 1:1000, 25 µl drops again

19. Incubate for 15 minutes at 37 °C.
20. Wash again and put on 9 µl mowiol drops
21. Push coverslip lightly into the mowiol with the tweezers
22. Remove unnecessary fluoromont/mowiol with paper
23. Wait overnight at 4 °C
24. Store at 4 °C

8.8 Treating cells with ZSTK

1. Plate cells on coverslips, let adhere overnight, as in 8.2 steps 1 to 2.
2. Prepare ZSTK: 1.2 µl of the aliquote in 12 ml of medium
3. Remove medium from wells
4. Wash with PBS
5. Add medium and ZSTK
6. Incubate at 37 °C for 2 hours
7. Proceed with fixing (8.2)

List of Figures

Bibliography

[1] B. Alberts, A. Johnson, J. Lewis, M. Raff, K. Roberts, and P. Walter. *Molecular Biology Of The Cell, Fifth Edition*. Garland Science, 2008.

[2] Fred Bunz. *Principles of Cancer Genetics*. Springer Science and Business Media, 2008.

[3] L. C. Cantley. The Phosphoinositide 3-Kinase Pathway. *Science*, 296(5573):1655–1657, may 2002.

[4] Etienne Caron, Samik Ghosh, Yukiko Matsuoka, Dariel Ashton-Beaucage, Marc Therrien, Sébastien Lemieux, Claude Perreault, Philippe P Roux, and Hiroaki Kitano. A comprehensive map of the mTOR signaling network. *Mol Syst Biol*, 6, dec 2010.

[5] A Carracedo and P P Pandolfi. The PTEN–PI3K pathway: of feedbacks and cross-talks. *Oncogene*, 27(41):5527–5541, sep 2008.

[6] Arkaitz Carracedo, Li Ma, Julie Teruya-Feldstein, Federico Rojo, Leonardo Salmena, Andrea Alimonti, Ainara Egia, Atsuo T. Sasaki, George Thomas, Sara C. Kozma, Antonella Papa, Caterina Nardella, Lewis C. Cantley, Jose Baselga, and Pier Paolo Pandolfi. Inhibition of mTORC1 leads to MAPK pathway activation through a PI3K-dependent feedback loop in human cancer. *Journal of Clinical Investigation*, aug 2008.

[7] Daniel A. Charlebois, Gábor Balázsi, and Mads Kærn. Coherent feedforward transcriptional regulatory motifs enhance drug resistance. *Phys. Rev. E*, 89(5), May 2014.

[8] N. Davoudzadeh, M. Tafazoli, and M.R. Sayeh. All-optical proteretic (reversed-hysteretic) bi-stable device. *Optics Communications*, 331:306–309, nov 2014.

[9] Yoh Dobashi, Yasutaka Watanabe, Chihiro Miwa, Sakae Suzuki, and Shinichiro Koyama. Mammalian target of rapamycin: a central node of complex signaling cascades. *Int J Clin Exp Pathol*, 4(5):476–495, 2011.

[10] James E Ferrell. Tripping the switch fantastic: how a protein kinase cascade can convert graded inputs into switch-like outputs. *Trends in Biochemical Sciences*, 21(12):460–466, dec 1996.

[11] James E Ferrell. Self-perpetuating states in signal transduction: positive feedback, double-negative feedback and bistability. *Current Opinion in Cell Biology*, 14(2):140–148, Apr 2002.

[12] James E. Ferrell and Wen Xiong. Bistability in cell signaling: How to make continuous processes discontinuous, and reversible processes irreversible. *Chaos*, 11(1):227, 2001.

[13] K. G. Foster and D. C. Fingar. Mammalian Target of Rapamycin (mTOR): Conducting the Cellular Signaling Symphony. *Journal of Biological Chemistry*, 285(19):14071–14077, mar 2010.

[14] T F Franke. PI3K/Akt: getting it right matters. *Oncogene*, 27(50):6473–6488, oct 2008.

[15] David A. Fruman and Christian Rommel. PI3k and cancer: lessons, challenges and opportunities. *Nature Reviews Drug Discovery*, 13(2):140–156, jan 2014.

[16] A. Goldbeter and D. E. Koshland. Sensitivity amplification in biochemical systems. *Quart. Rev. Biophys.*, 15(03):555, aug 1982.

[17] K Held, H Leeb, C Lemell, and H M"uller. Skriptum zur vu 138.094 'numerische methoden und simulation'. TU Wien, Mrz 2015.

[18] Bryan T. Hennessy, Debra L. Smith, Prahlad T. Ram, Yiling Lu, and Gordon B. Mills. Exploiting the PI3k/AKT pathway for cancer drug discovery. *Nat Rev Drug Discov*, 4(12):988–1004, dec 2005.

[19] M. Christine Hollander, Gideon M. Blumenthal, and Phillip A. Dennis. PTEN loss in the continuum of common cancers, rare syndromes and mouse models. *Nature Reviews Cancer*, 11(4):289–301, apr 2011.

[20] Tweeny R Kau, Frank Schroeder, Shivapriya Ramaswamy, Cheryl L Wojciechowski, Jean J Zhao, Thomas M Roberts, Jon Clardy, William R

Sellers, and Pamela A Silver. A chemical genetic screen identifies inhibitors of regulated nuclear export of a forkhead transcription factor in PTEN-deficient tumor cells. *Cancer Cell*, 4(6):463–476, dec 2003.

[21] James Keener and James Sneyd. *Mathematical Physiology*, volume 8/1. Springer-Verlag New York, 2 edition, 2009.

[22] J. Koolman, K.-H. Roehm, and J. Wirth. *Color Atlas of Biochemistry, Second Edition*. Georg Thieme Verlag, 2005.

[23] D. Koshland, A Goldbeter, and J. Stock. Amplification and adaptation in regulatory and sensory systems. *Science*, 217(4556):220–225, jul 1982.

[24] Nick R. LESLIE and C. Peter DOWNES. PTEN function: how normal cells control it and tumour cells lose it. *Biochem. J.*, 382(1):1–11, aug 2004.

[25] X. Z. Li, X. H. Wei, R. Skomski, and D. J. Sellmyer. Structure and magnetism of Co:CoO core-shell nanoclusters. *Journal of Nanoparticle Research*, 12(3):789–794, oct 2009.

[26] J. E. Lisman. A mechanism for memory storage insensitive to molecular turnover: a bistable autophosphorylating kinase. *Proceedings of the National Academy of Sciences*, 82(9):3055–3057, may 1985.

[27] Pixu Liu, Hailing Cheng, Thomas M. Roberts, and Jean J. Zhao. Targeting the phosphoinositide 3-kinase pathway in cancer. *Nature Reviews Drug Discovery*, 8(8):627–644, aug 2009.

[28] Christopher Louizos, Jaime A Yáñez, M Laird Forrest, and Neal M Davies. Understanding the Hysteresis Loop Conundrum in Pharmacokinetic/Pharmacodynamic Relationships. *Journal of Pharmacy & Pharmaceutical Sciences*, 17(1):34–91, 2014.

[29] Moulun Luo, Paul Langlais, Zhengping Yi, Natalie Lefort, Elena A. De Filippis, Hyonson Hwang, Christine Y. Christ-Roberts, and Lawrence J. Mandarino. Phosphorylation of human insulin receptor substrate-1 at serine 629 plays a positive role in insulin signaling. *Endocrinology*, 148(10):4895–4905, oct 2007.

[30] Brendan D. Manning and Lewis C. Cantley. AKT/PKB Signaling: Navigating Downstream. *Cell*, 129(7):1261–1274, jun 2007.

[31] David G Míguez. Network nonlinearities in drug treatment. *Interdiscip Sci*, 5(2):85–94, June 2013.

[32] David G Míguez, William Senapedis, and Juan Carlos Martinez-Garcia. Nonlinearities in the akt signaling pathway regulate the response of cancer cells to anti-tumor inhibitors. *Manuscript in preparation*, 2014.

[33] Jacques Monod and Francois Jacob. General Conclusions: Teleonomic Mechanisms in Cellular Metabolism, Growth, and Differentiation. *Cold Spring Harb Symp Quant Biol*, 26(26):389–401, 1961.

[34] J. D. Murray. *Mathematical Biology I: An Introduction*, volume 17 of *Interdisciplinary Applied Mathematics*. Springer New York, 2002.

[35] J. Paul Robinson PhD, Jennifer Sturgis BS, and George L. Kumar PhD. Chapter 10: Immunofluorescence. *IHC Staining Methods, Fifth edition*.

[36] Leonardo Salmena, Arkaitz Carracedo, and Pier Paolo Pandolfi. Tenets of PTEN Tumor Suppression. *Cell*, 133(3):403–414, may 2008.

[37] Michael P. Scheid, James R. Woodgett, and James R. Woodgett. PKB/AKT: FUNCTIONAL INSIGHTS FROM GENETIC MODELS. *Nature Reviews Molecular Cell Biology*, 2(10):760–768, oct 2001.

[38] Gang Song, Gaoliang Ouyang, and Shideng Bao. The activation of Akt/PKB signaling pathway and cell survival. *Journal of Cellular and Molecular Medicine*, 9(1):59–71, jan 2005.

[39] S. H. Strogatz. *Nonlinear Dynamics and Chaos*. Westview Press, Cambridge, MA, 1994.

[40] F. Vazquez, S. Matsuoka, W. R. Sellers, T. Yanagida, M. Ueda, and P. N. Devreotes. Tumor suppressor PTEN acts through dynamic interaction with the plasma membrane. *Proceedings of the National Academy of Sciences*, 103(10):3633–3638, feb 2006.

[41] Francisca Vazquez and William R Sellers. The PTEN tumor suppressor protein: an antagonist of phosphoinositide 3-kinase signaling. *Biochimica et Biophysica Acta (BBA) - Reviews on Cancer*, 1470(1):M21–M35, feb 2000.

[42] Igor Vivanco and Charles L. Sawyers. The phosphatidylinositol 3-Kinase–AKT pathway in human cancer. *Nat. Rev. Cancer.*, 2(7):489–501, jul 2002.

[43] X.-H. Wei, R. Skomski, Z.-G. Sun, and D. J. Sellmyer. Proteresis in Co:CoO core-shell nanoclusters. *J. Appl. Phys.*, 103(7):07D514, 2008.

[44] S.-i. Yaguchi, Y. Fukui, I. Koshimizu, H. Yoshimi, T. Matsuno, H. Gouda, S. Hirono, K. Yamazaki, and T. Yamori. Antitumor Activity of ZSTK474, a New Phosphatidylinositol 3-Kinase Inhibitor. *JNCI Journal of the National Cancer Institute*, 98(8):545–556, apr 2006.